NASA/TM—2002-211512

A Flow Solver for Three-Dimensional DRAGON Grids

Meng-Sing Liou
Glenn Research Center, Cleveland, Ohio

Yao Zheng
Taitech, Inc., Cleveland, Ohio

May 2002

The NASA STI Program Office . . . in Profile

Since its founding, NASA has been dedicated to the advancement of aeronautics and space science. The NASA Scientific and Technical Information (STI) Program Office plays a key part in helping NASA maintain this important role.

The NASA STI Program Office is operated by Langley Research Center, the Lead Center for NASA's scientific and technical information. The NASA STI Program Office provides access to the NASA STI Database, the largest collection of aeronautical and space science STI in the world. The Program Office is also NASA's institutional mechanism for disseminating the results of its research and development activities. These results are published by NASA in the NASA STI Report Series, which includes the following report types:

- TECHNICAL PUBLICATION. Reports of completed research or a major significant phase of research that present the results of NASA programs and include extensive data or theoretical analysis. Includes compilations of significant scientific and technical data and information deemed to be of continuing reference value. NASA's counterpart of peer-reviewed formal professional papers but has less stringent limitations on manuscript length and extent of graphic presentations.

- TECHNICAL MEMORANDUM. Scientific and technical findings that are preliminary or of specialized interest, e.g., quick release reports, working papers, and bibliographies that contain minimal annotation. Does not contain extensive analysis.

- CONTRACTOR REPORT. Scientific and technical findings by NASA-sponsored contractors and grantees.

- CONFERENCE PUBLICATION. Collected papers from scientific and technical conferences, symposia, seminars, or other meetings sponsored or cosponsored by NASA.

- SPECIAL PUBLICATION. Scientific, technical, or historical information from NASA programs, projects, and missions, often concerned with subjects having substantial public interest.

- TECHNICAL TRANSLATION. English-language translations of foreign scientific and technical material pertinent to NASA's mission.

Specialized services that complement the STI Program Office's diverse offerings include creating custom thesauri, building customized data bases, organizing and publishing research results . . . even providing videos.

For more information about the NASA STI Program Office, see the following:

- Access the NASA STI Program Home Page at ***http://www.sti.nasa.gov***

- E-mail your question via the Internet to help@sti.nasa.gov

- Fax your question to the NASA Access Help Desk at 301–621–0134

- Telephone the NASA Access Help Desk at 301–621–0390

- Write to:
  NASA Access Help Desk
  NASA Center for AeroSpace Information
  7121 Standard Drive
  Hanover, MD 21076

NASA/TM—2002-211512

A Flow Solver for Three-Dimensional DRAGON Grids

Meng-Sing Liou
Glenn Research Center, Cleveland, Ohio

Yao Zheng
Taitech, Inc., Cleveland, Ohio

National Aeronautics and
Space Administration

Glenn Research Center

May 2002

Acknowledgments

This work is supported under Turbomachinery and Combustion Technology, managed by Robert Corrigan, NASA Glenn Research Center. We thank R.V. Chima for providing the vane geometry of the annular cascade.

The Aerospace Propulsion and Power Program at
NASA Glenn Research Center sponsored this work.

Available from

NASA Center for Aerospace Information
7121 Standard Drive
Hanover, MD 21076

National Technical Information Service
5285 Port Royal Road
Springfield, VA 22100

Available electronically at http://gltrs.grc.nasa.gov/GLTRS

A Flow Solver for Three-Dimensional DRAGON Grids

Meng-Sing Liou
National Aeronautics and Space Administration
Glenn Research Center
Cleveland, Ohio 44135

Yao Zheng
Taitech, Inc.
Cleveland, Ohio 44135

Abstract

DRAGONFLOW is a flow solver devoted to the Computational Fluid Dynamics (CFD) simulation using the three-dimensional DRAGON grid technology. DRAGONFLOW is a program suite adopted and redesigned from two existing successful flow solvers OVERFLOW and USM3D. OVERFLOW is a Navier-Stokes code working with Chimera grid, and is used here to solve flow problems on the domain occupied by composite structured grids of a DRAGON grid. USM3D is characteristic-based scheme for steady solutions to the Navier-Stokes equations on unstructured tetrahedral grid, and is employed to pursue flow simulation over a collection of unstructured grids of a DRAGON grid.

DRAGON grid is constructed to be a combination of a Chimera grid and a collection of unstructured grids. In the DRAGONFLOW suite, both OVERFLOW and USM3D are presented in form of module libraries, and a master module controls the invoking of these individual modules. The alternating invoking of these solvers in each time step, and the immediate data exchange on the DRAGON grid interfaces, leads to a seamless coupling of these two solvers. This report includes essential aspects, programming structures, benchmark tests and numerical simulations.

1 Introduction

During the past decades, both structured and unstructured grid techniques have been extensively developed and applied to solution of various engineering problems. To deal with

situations in which complex geometry imposes considerable constraints and difficulties in generating grids, composite structured grid schemes and unstructured grid schemes currently are the two mainstream approaches.

In general, unstructured grid methods are considered to be more versatile and easier to adapt to complex geometries but less suitable for resolving viscous layers, while composite structured grid methods are considered to be more flexible to use efficient numerical algorithms and require less computer memory. Clearly, both methods complement each other on strengths and weaknesses. Hence, a method that properly employs a hybrid of structured and unstructured grids may prove to be fruitful. In fact some hybrid schemes have already appeared in the literature [7, 17, 18, 20] and have shown promising features.

The DRAGON grid [8, 13, 22], as a hybrid grid, is created by means of a Direct Replacement of Arbitrary Grid Overlapping by Nonstructured grid. The DRAGON grid scheme is an adaptation to the Chimera thinking. The Chimera grid is a composite structured grid, composing a set of overlapped structured grids, which are independently generated and body-fitted. The grid is of high quality and amenable for efficient solution schemes. However, the interpolation used in the overlapped region between grids introduces error, especially when a sharp-gradient region is encountered [10, 19]. The DRAGON grid scheme is capable of completely eliminating the interpolation and preserving the flux conservation property. It adapts and maximizes the advantages of both structured and unstructured grids, while at the same time it eliminates the weaknesses of the Chimera scheme and minimizes the memory requirement associated with the unstructured grid.

We have developed an extension of the DRAGON grid technology into three-dimensional space [15, 16, 21, 22]. The present work is to develop a flow solver devoted to the Computational Fluid Dynamics (CFD) simulation using DRAGON grid technology in the three-dimensional space [15, 16, 21]. The resulting program suite is named as DRAGONFLOW. It is the result of integrating works of other researchers, and it is adopted and redesigned from two existing successful flow solvers OVERFLOW [1] and USM3D [4, 5]. OVERFLOW is a Navier-Stokes code working with Chimera grid, and is used here to solve flow problems on the domain occupied by composite structured grids of a DRAGON grid. USM3D solves Navier-Stokes equations on an unstructured tetrahedral grid, and is employed to perform flow simulation over a collection of unstructured grids of a DRAGON grid.

The present work is written to define rules over the programming practice employed during the development of DRAGONFLOW. This introductory document includes essential aspects, programming structures, benchmark tests and numerical simulations.

2 Solution Scheme

2.1 Governing Equations

The time-dependent compressible Navier-Stokes equations given by Equation (1), in an integral form over an arbitrary control volume Ω, are solved:

$$\int_{\Omega} \frac{\partial \mathbf{U}}{\partial t} d\upsilon + \int_{\partial\Omega} \vec{\mathbf{F}} \bullet d\vec{S} = 0, \tag{1}$$

where the conservative-variable vector $\mathbf{U} = (\rho, \rho u, \rho v, \rho w, \rho e_t)^T$, with the specific total energy $e_t = e + |\vec{V}|^2/2 = h_t - p/\rho$. The flux vector $\vec{\mathbf{F}}$ includes both the inviscid and viscous fluxes, in which the turbulence variables are also included. We denote with an overhead arrow the vector quantities expressed in terms of Cartesian coordinates.

2.2 Flux Splitting

Based on the cell-centered finite volume method, the governing equations are semi-discretized. We use the flux scheme AUSM$^+$, described in full detail in [11], to express the numerical inviscid flux at the cell faces. The basic idea of AUSM$^+$ follows that of its predecessor, AUSM [14], but has substantial improvements. The AUSM$^+$, incurring negligible additional cost over the earlier AUSM scheme, allows exact capture of a normal shock by using a suitably chosen interface speed of sound, yields a smoother solution by utilizing higher-order polynomials, and often results in a faster convergence rate.

The semi-discretized form, describing the time rate of change of $\mathbf{U}$ in Ω via balance of fluxes through all enclosing faces, $\vec{S}_l, l = 1, \cdots, LX$, independent of whether they are in the structured or unstructured grid regions, can be cast as

$$\int_{\Omega} \frac{\partial \mathbf{U}}{\partial t} d\upsilon + \sum_{l=1}^{LX} \vec{\mathbf{F}}_l \bullet \vec{S}_l = \int_{\Omega} \frac{\partial \mathbf{U}}{\partial t} d\upsilon + \sum_{l=1}^{LX} \mathbf{F}_{nl} |\vec{S}_l| = 0. \tag{2}$$

Noting that the flux terms account for only normal components of the flux at the face, $\mathbf{F}_{nl} = \vec{\mathbf{F}}_l \bullet \vec{n}_l$ where $\vec{n}_l$ is the unit normal vector of $\vec{S}_l$. The task is then to represent the numerical flux at the cell interface $\vec{S}_l$, which straddles cells denoted by subscripts "L" and "R". The AUSM$^+$ scheme gives the numerical flux in the following expression.

$$\mathbf{F}_{nl} = M_l \frac{a_l}{2}(\mathbf{\Phi}_L + \mathbf{\Phi}_R) - |M_l| \frac{a_l}{2} \Delta\mathbf{\Phi} + \mathbf{P}_{nl}. \tag{3}$$

We remark that there is enough freedom for defining the interface speed of sound a_l so that certain criteria are met [11, 12]. An interesting notion is the so-called numerical speed of sound, which is introduced to handle low Mach number flows and later is extended to the multiphase flows [12]. The interface Mach number M_l is an important variable and defined in the following steps.

1. Project velocity vectors at the cell centers, "L" and "R", to $\vec{S}_l$,

$$V_L = \vec{V}_L \bullet \vec{n}_l, \quad V_R = \vec{V}_R \bullet \vec{n}_l. \tag{4}$$

2. Define the corresponding Mach numbers,

$$M_L = \frac{V_L}{a_l}, \quad M_R = \frac{V_R}{a_l}, \tag{5}$$

3. Define the interface convective Mach number by writing

$$M_l = \mathcal{M}^+_{(4)}(M_L) + \mathcal{M}^-_{(4)}(M_R), \tag{6}$$

where the formulas for $\mathcal{M}^{\pm}_{(4)}$ are expressed in terms of eigenvalues of the nonlinear waves, $M+1$ and $M-1$ [11].

$$\mathcal{M}^{\pm}_{(4)}(M) = \begin{cases} \frac{1}{2}(M \pm |M|), & \text{if } |M| \geq 1, \\ \mathcal{M}^{\pm}_{(2)}(1 \mp 2\mathcal{M}^{\mp}_{(2)}), & \text{otherwise,} \end{cases} \tag{7}$$

where

$$\mathcal{M}^{\pm}_{(2)}(M) = \pm\frac{1}{4}(M \pm 1)^2. \tag{8}$$

4. Define the interface pressure p_l in terms of the above-defined Mach numbers,

$$p_l = \mathcal{P}^+_{(5)}(M_L)p_L + \mathcal{P}^-_{(5)}(M_R)p_R \tag{9}$$

where similarly we use the following polynomials,

$$\mathcal{P}_{(5)}{}^{\pm}(M) = \begin{cases} \frac{1}{2M}(M \pm |M|), & \text{if } |M| \geq 1, \\ \mathcal{M}^{\pm}_{(2)}[(\pm 2 - M) \mp 3M\mathcal{M}^{\mp}_{(2)}], & \text{otherwise.} \end{cases} \tag{10}$$

Then, we get

$$\mathbf{P}_{nl} = p_l \begin{pmatrix} 0 \\ n_{lx} \\ n_{ly} \\ n_{lz} \\ 0 \end{pmatrix}. \tag{11}$$

5. Assemble the interface numerical flux by inserting $(M_l, \mathbf{P}_{nl})$ in Eq. (3).

2.3 Flow Solvers

As mentioned before, the flow code DRAGONFLOW is made up of two well-validated NASA codes, OVERFLOW [1] and USM3D [5], which are respectively structured- and unstructured-grid codes. We have spent a significant effort to add an interface and modify both codes, more so for the OVERFLOW code. The interested readers should consult with

the cited references for details of either code. The details on implementing the DRAGON-FLOW code are to be addressed in Section 4. Nonetheless, there are differences between these codes that warrant concerns and cares when combining them into the present framework, such as time integration schemes, order of spatial discretizations, and choice of turbulence models.

A spatial-factored implicit algorithm is employed in the OVERFLOW code, while a point implicit one in the USM3D code. Since we are only interested in seeking steady state solutions, the differences of convergence rate due to the incompatibility between the structured and unstructured grid regions can be tolerated. However, if unsteady solutions are of interest, this difficulty can be overcome by a dual time integration approach in which the solution within each physical time step will be iterated to achieve convergence. This subject is left for a future research.

As for the spatial discretization, there is inconsistency in the order of accuracy in that a third-order and a second-order accurate schemes are used respectively in the structured grid-based and unstructured grid-based codes. But in both cases a similar limiter function is applied. We use the aforementioned flux scheme AUSM$^+$ to express the inviscid flux at the cell faces in both the OVERFLOW and USM3D codes. Also, the viscous fluxes are approximated, as usual, by a centered scheme.

3 Data Communication through Grid Interface

3.1 Generic Concept

In the Chimera method, communication through grid interfaces is made through the hole boundary or the outer boundary. Since the interface treatment methods are not necessarily satisfying any form of conservative constraints, the solutions on overlaid grids are often mismatched with each other. More seriously, this may ultimately lead to spurious or incorrect solutions, especially when a shock wave or high-gradient region passes through boundaries of overlaid grids, as will be seen later.

For the DRAGON grid, conservation laws are solved on the same basis on both the structured and unstructured grids. Figure 1 shows an interface connecting both structured and unstructured grids, assuming the cell center scheme is used. As described earlier, the numerical fluxes, evaluated at the cell interface, are based on the conditions of neighboring cells (denoted as L and R cells, respectively). For the unstructured grid, the interface flux $\mathbf{F}_{nl}$, will be evaluated using the structured-cell value as the right (R) state and the unstructured-cell value as the left (L) state. Consequently, the interface fluxes, which have been evaluated for the unstructured grid, can now be directly applied in computing the cell volume residuals for the structured grid.

Thus, the data communication through grid interfaces in the DRAGON grid guarantees satisfying of the conservation laws. It is considered seamless in the sense that no manipulation of data, which introduces uncertainties, is required, and the solution is obtained on the same basis for both structured and unstructured grid regions. Consequently this strictly enforces the conservation property locally and globally.

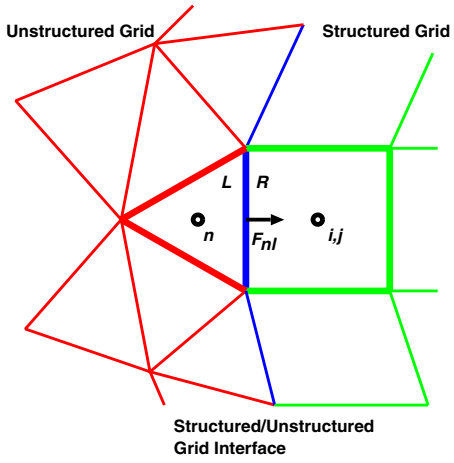

Figure 1: Fluxes at the cell face connecting the structured and unstructured grids.

3.2 Fictitious Structured Grids

In Figure 1, the cell center scheme is assumed for both structured and unstructured grids. However, the OVERFLOW code used in the structured grid regions is developed based on a nodal-based scheme, where the flow variables are solved and stored at the grid points, rather than being offset to the center of the cells defined by the grid points. The surface of the unstructured grids within interfacial areas between the two types of grids could not match a surface described by nodes in the structured grids, in order to establish reasonable data communication through grid interfaces. For the DRAGONFLOW code, special treatment has been proposed to tackle the difficulty associated with the difference between cell-based and node-based schemes. This can be neatly resolved by a novel use of fictitious structured grids based on the original structured grids.

From a structured grid with $l \times m \times n$ nodes, an artificial grid with $(l+1) \times (m+1) \times (n+1)$ nodes can be constructed by means of introducing middle nodes between original nodes. It is clear that the new grid is shifted from the original one by a half cell size in the interior of the original grid. This new grid is referred to as a fictitious grid, and the associated nodes are named as fictitious nodes. Figure 2 gives an illustration of the fictitious grid. Cell center (j,k), which is node $(j,k)_o$ of the original grid, is surrounded by nodes $(j,k)_f$, $(j+1,k)_f$, $(j+1,k+1)_f$ and $(j,k+1)_f$ of the fictitious grid. Subscripts o and f denote "original" and "fictitious" grids, respectively.

3.3 Establishing DRAGON Grid Interfaces

It is obvious that the faces described by the fictitious nodes are the faces of finite volumes centered at the original nodes. For the fictitious grids, if we mimic the gridding method of DRAGON grids based on the original structured grids, as proposed in Reference [22], then we can generate a DRAGON grid based on the fictitious grids. Moreover, the DRAGON interfacial boundary nodes of the unstructured grid coincide with the corresponding nodes

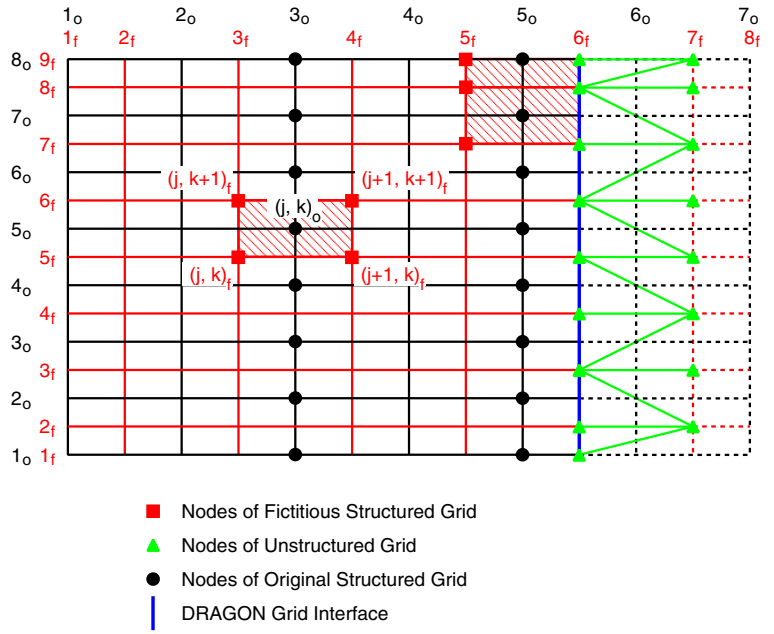

Figure 2: Diagram of a fictitious grid associated with its original structured grid.

on the fictitious grid. Because the numerical fluxes are still conservative in the DRAGON grid interface, the conservation property will not be affected by means of using a fictitious grid.

During the creation of the DRAGON grid based on the fictitious grids, IBLANK values for the fictitious grids can be automatically specified, taking into account the IBLANK values of the original grids. A fictitious node is specified 1 as its IBLANK value, if and only if there is an original node nearby with IBLANK value 1. According to this convention, a special case depicted in Figure 3 should be taken care of.

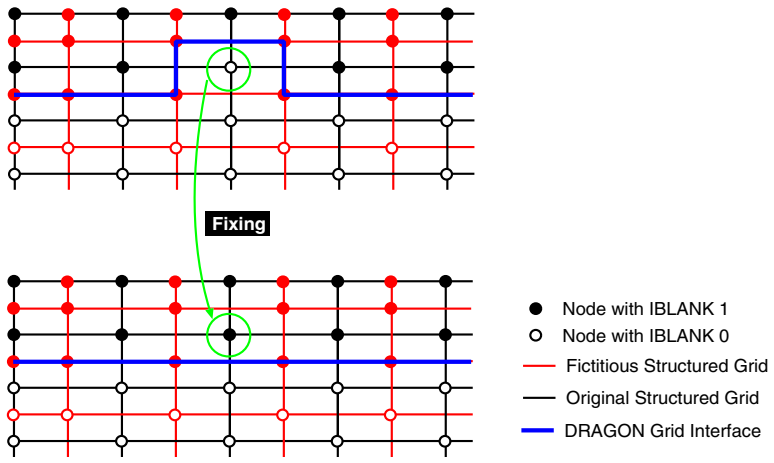

Figure 3: Special case to fix IBLANK values on the original structured grid.

The faces of DRAGON grid interface are constructed from certain faces of the finite volumes centered at the original nodes. For an original node of interest, there are six possible faces, which could become faces of the DRAGON grid interface. Figure 4 illustrates the numbering systems of the original grid, fictitious grid and flux definition, given Faces A and B as possible faces of the DRAGON grid interface, within a frame of a two-dimension problem. In this case, Faces A and B are defined as $(j,k;-1)$ and $(j,k;1)$, where ± 1 denotes the directions of the face. For Face A (idir $=-1$), $(j,k;-1)$ represents the index of cell center j_o, flux $(j-1)_{fl}$ at the $j-1$ face and the fictitious grid index j_f. While for Face B (idir $=1$), $(j,k;1)$ represents the index of cell center j_o, flux j_{fl} at the j face and the fictitious grid index $(j+1)_f$. Generally, for three-dimensional cases, the notation of face directions is given in Figure 5.

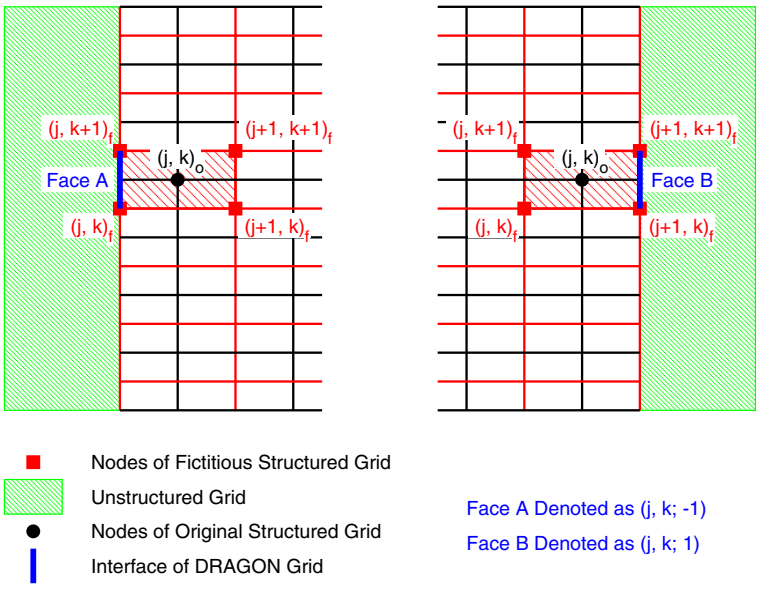

Figure 4: Diagram of 2D DRAGON grid interfaces.

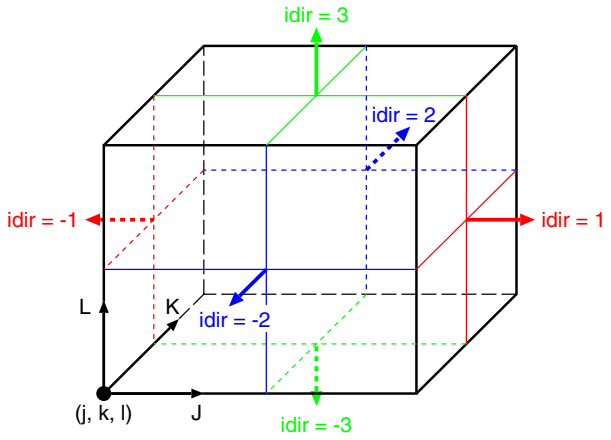

Figure 5: Notation of face directions of 3D DRAGON grid interfaces.

3.4 Nodal Variables near DRAGON Grid Interfaces

In the DRAGONFLOW procedure, values of nodal variables of structured grids near the interfaces are passed to the counterpart in the side of unstructured grids. These values are used to compute flux values on the interfaces. Therefore, the information from the side of structured grids contributes to the evolution of the solution in the unstructured grid regions. On the other hand, the fluxes computed are passed to the OVERFLOW to influence the solution in the structured grid regions.

Figure 6 is a diagram of passing Q values from structured to unstructured grids. The corresponding values are stored in Arrays Q_b and Q_{gh} in the USM3D part. It should be mentioned that Q values in the OVERFLOW and USM3D parts are in terms of conservative variables and primitive ones, respectively. A conversion has been conducted when Q values are passed from structured to unstructured grids. Q_1, Q_2, Q_b and Q_{gh} in Figure 6 are all primitive. As every face of the interface from the structured grid side is split into at least two faces in the unstructured grid side, Q_b values of several unstructured grid elements are identical. And same situation occurs for Q_{gh} values. When the structured grids are distorted very much near the DRAGON grid interfaces, the accuracy of assigning Q_b and Q_{gh} values in this way is lowered, referring to Figure 7. This is a main area that accuracy could be affected.

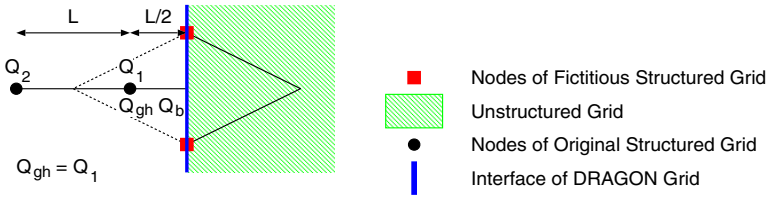

Figure 6: Diagram of Q values from structured to unstructured grids.

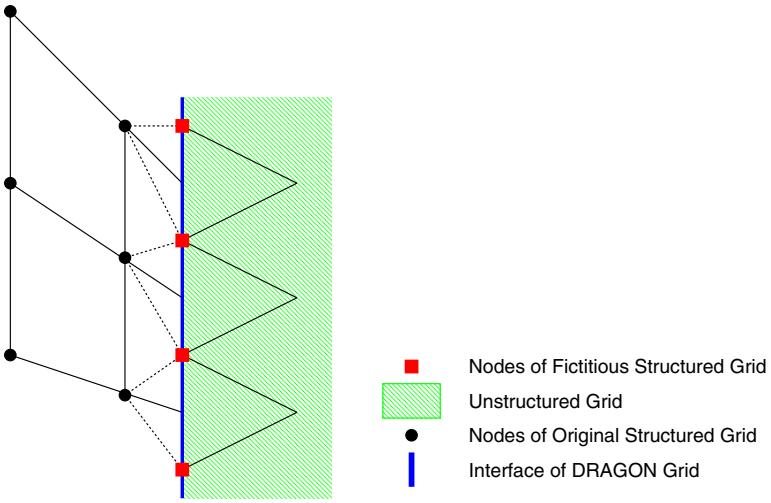

Figure 7: Diagram of a neighborhood of the DRAGON grid interface, when the structured grid is distorted.

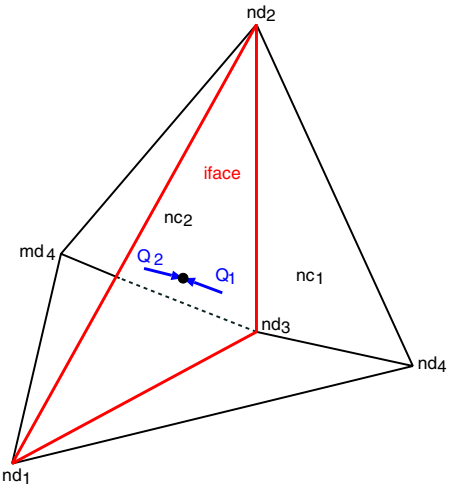

Figure 8: Diagram of Q values in an unstructured grid.

During the flux calculation in the USM3D part, high-order spatial differencing is used for high-order cases. Referring to Figures 8 and 9, Q value on Face f_{123}, that is, $Q_{f_{123}}$, can be deduced by Equations 12 and 13, where Q_c denotes Q value at the center of the element.

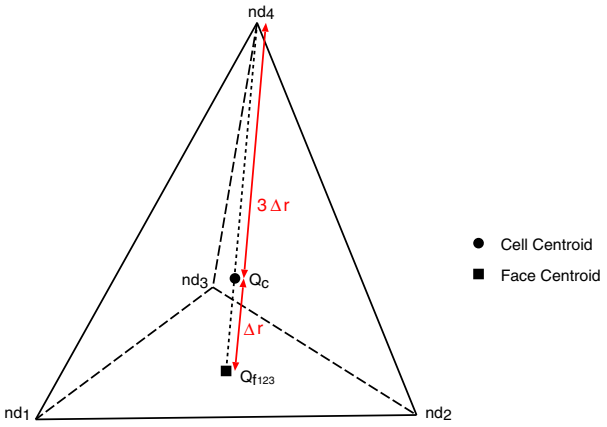

Figure 9: Diagram of Q_{f123} calculation.

$$\nabla Q_c \cdot \mathbf{\Delta r} = \frac{\partial Q}{\partial r}\Delta r = \left[\frac{\frac{1}{3}(Q_{nd_1} + Q_{nd_2} + Q_{nd_3}) - Q_{nd_4}}{4\Delta r}\right]\Delta r \tag{12}$$

$$Q_{f_{123}} = Q_c + \text{limiter}\{\frac{1}{12}(Q_{nd_1} + Q_{nd_2} + Q_{nd_3}) - Q_{nd_4}\} \tag{13}$$

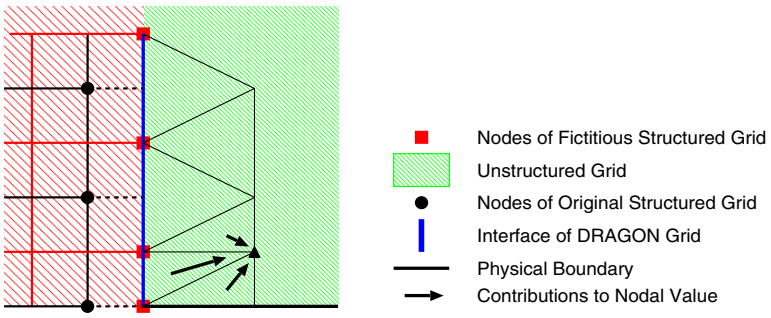

Figure 10: Contributions to interior nodal values.

Table 1: Various averaging schemes for nodal values.

lapavg	Descriptions
-1	Pseudo-Laplacian averaging on interior nodes; Inverse-distance averaging on boundary nodes. Boundary nodal values have no contributions from values of interior cell centers.
0	Inverse-distance averaging to all nodes. Boundary nodal values have no contributions from values of interior cell centers.
1	Pseudo-Laplacian averaging to all nodes. Boundary nodal values are computed from ghost cells and all interior cells sharing the boundary nodes.
2	Revised inverse-distance averaging, same as that of lapavg=3, at the first step. From the second step, set lapavg to 1.
3	Inverse-distance averaging to all nodes. Boundary nodal values are computed from ghost cells and all interior cells sharing the boundary nodes.

We treat the DRAGON grid interface as a boundary, however routine `UBC` in the USM3D code does nothing with this special boundary. Routine `QNODE` in the USM3D part computes distance-averaged Q values of node points, and it remains almost the same even after the addition of the special boundary type. Table 1 lists five *lapavg* values for the `QNODE` routine. Figures 10 and 11 show the schemes of calculating contributions to interior and boundary nodal values.

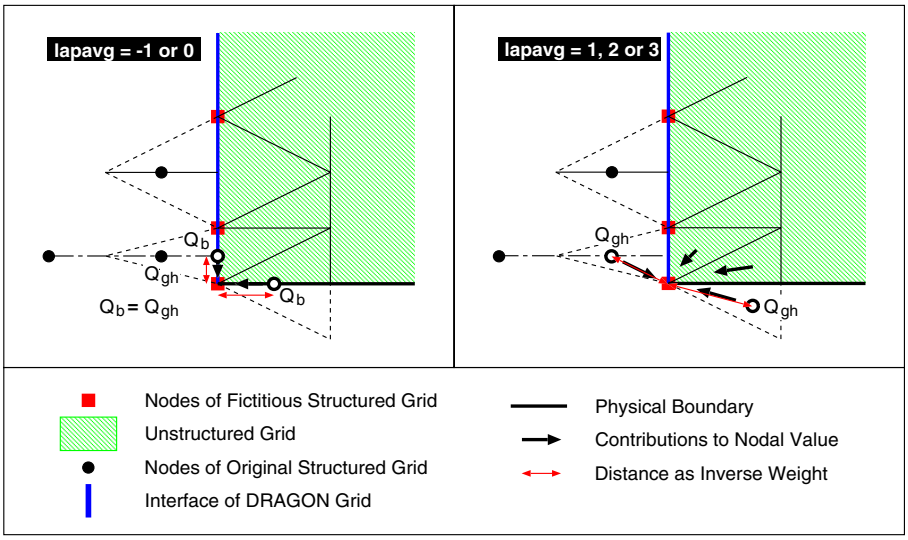

Figure 11: Contributions to boundary nodal values.

Nodal value Q_n may have slight influence on dtv(*) in subroutine `UCTIME`, when $dt \leq 0$. It will results in changes in fluxes and resid(*) in subroutine `AUSM`, when iorder ≥ 2. It will results in changes in viscous fluxes in subroutine `GFLUX`, when ivisc > 0.

3.5 Flux Values near DRAGON Grid Interfaces

As mentioned before, the fluxes calculated based on the information on tetrahedral elements are used to update corresponding fluxes associated with the structured grids, due to the requirement of flux conservation on the DRAGON grid interfaces. Therefore, topology relationship between the two types of grids near the DRAGON grid interfaces is established before hand, and Figure 12 illustrates this corresponding relation.

In the OVERFLOW part, nodal Q values and fluxes are stored in the way as shown in Figure 13. When periodic or annular periodic boundary conditions are encountered, attention should be paid on the Q values near boundaries.

For the three-dimensional case, all the fluxes are arranged in $J-K$ planes for J-direction fluxes (in Files `reuj.F` and `reuj2.F`), $J-K$ planes for K-direction fluxes (in Files `reuk.F` and `reuk2.F`), and $J-L$ planes for L-direction fluxes (in Files `reul.F` and `reul2.F`). Originally, there are $(n_j-1)\times(n_k)\times(n_l-2)$ J-direction fluxes, $(n_j)\times(n_k-1)\times(n_l-2)$ K-direction fluxes, and $(n_j)\times(n_k-2)\times(n_l-1)$ L-direction fluxes. Referring to Figure 14,

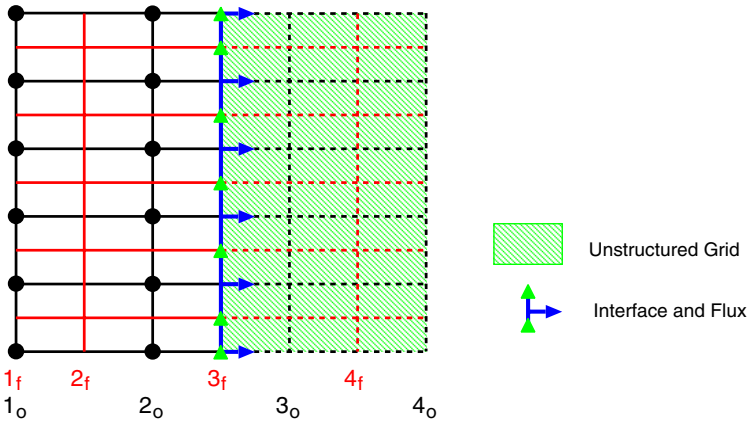

Figure 12: Fluxes concerned on the interface between the fictitious and unstructured grids.

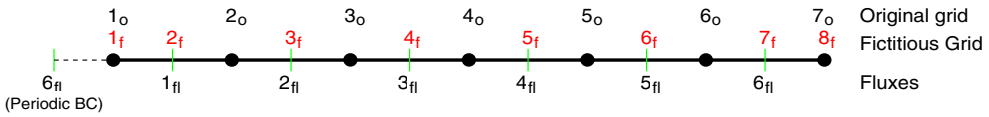

Figure 13: Flux notation with respect to the original and fictitious structured grids.

some fluxes shown as shaded will not be updated, according to the design of the OVERFLOW code. Therefore, there are only $(n_j - 1) \times (n_k - 2) \times (n_l - 2)$ J-direction fluxes, $(n_j - 2) \times (n_k - 1) \times (n_l - 2)$ K-direction fluxes, and $(n_j - 2) \times (n_k - 2) \times (n_l - 1)$ L-direction fluxes, which are to be updated.

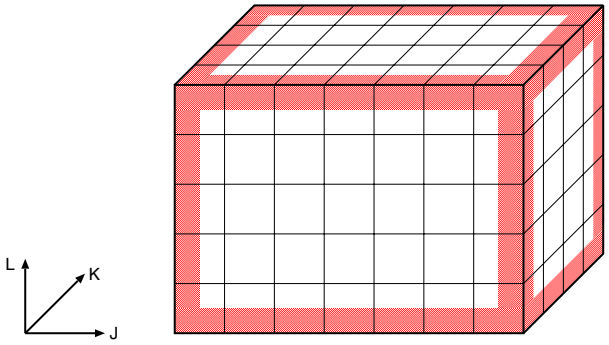

Figure 14: Diagram of fluxes associated with the original structured grid that are not updated.

For the OVERFLOW code, the Q value on node j is denoted as Q_j, and the corresponding fluxes near node j are denoted as F_{j-1} and F_j (Refer to Figure 15). For the first-order flux splitting/upwind option, there is

$$F_j = f(Q_j, Q_{j+1}), \; F_{j-1} = f(Q_{j-1}, Q_j). \tag{14}$$

For the higher order cases (*ie.* second- and third-order), there exists interpolated/limited states

$$Q_j^* = \text{Int}(Q_{j-1}, Q_j, Q_{j+1}), \tag{15}$$

so that

$$F_j = f(Q_j^*, Q_{j+1}^*),\ F_{j-1} = f(Q_{j-1}^*, Q_j^*). \tag{16}$$

Various forms for higher order interpolations and limiter functions are abundant in literature; the one used in the OVERFLOW code is the third-order MUSCL scheme with the Koren's limiter [9]. Figure 15 depicted this generic scheme of flux calculation, in terms of the nodal values used. As Q values at five nodes are taken into account, for the flux computation for the third-order option, it is necessary to construct and correct Q values at certain nodes with IBLANK value 0. By circling the targeted nodes, Figure 16 shows the correction of nodal values associated.

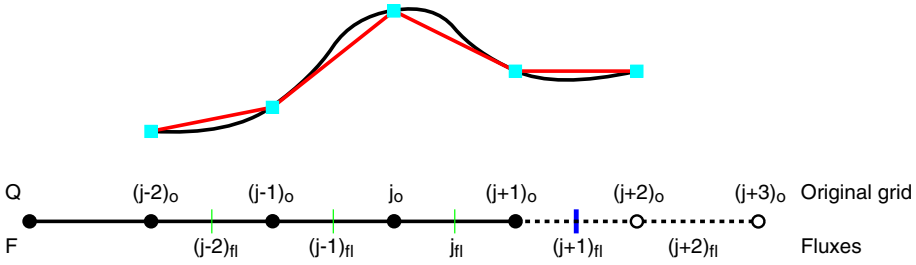

Figure 15: Calculation of fluxes on structured grids.

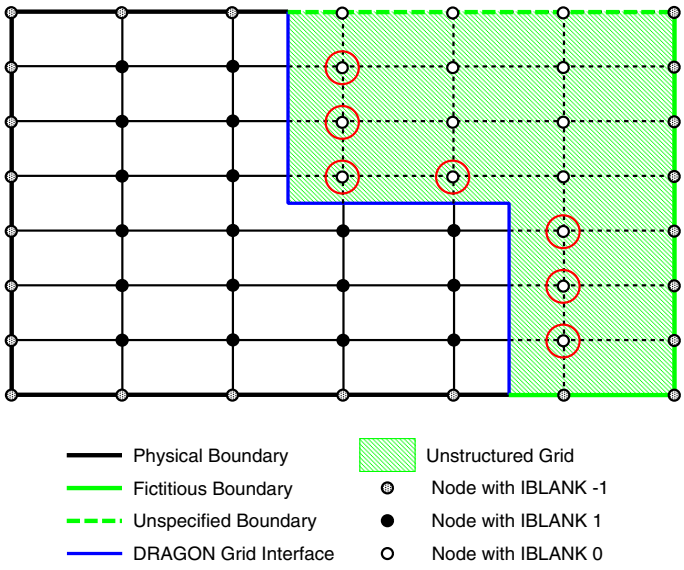

Figure 16: Correction of some nodal values on the structured grids.

4 Implementation of the Solver

4.1 Programming Philosophy

The adoption of OVERFLOW and USM3D codes for the DRAGON grid is based on the concept of domain splitting. A DRAGON grid is dealt with as a combination of a Chimera grid and a collection of unstructured grids. In the DRAGONFLOW suite, both OVERFLOW and USM3D are presented in form of module libraries, and a master module controls the invoking of these individual modules. The alternative invoking of these solvers in each time step, and the immediate data exchange on the DRAGON grid interfaces, leads to a seamless coupling of these two solvers. Figure 17 depicts the flow chart of the DRAGONFLOW suite. A significant effort has been made to add an interface and modify both codes, more so on the OVERFLOW code.

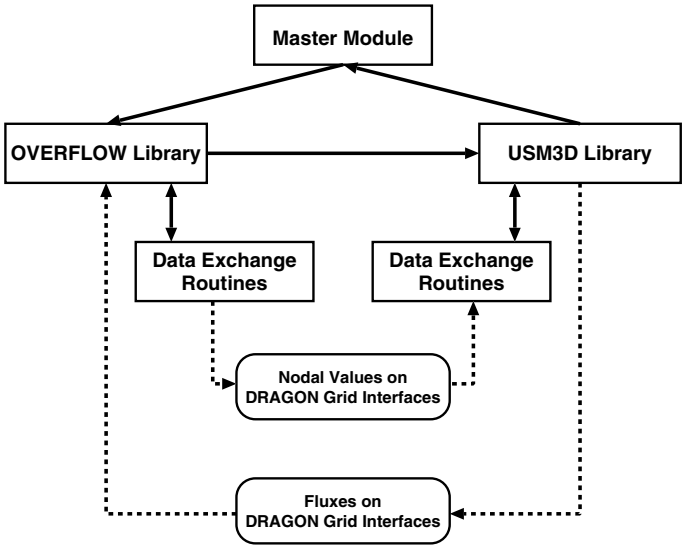

Figure 17: Flowchart of the DRAGONFLOW procedure.

The DRAGONFLOW code keeps the structure of the OVERFLOW code. Directory `chimera` has been renamed as `dragon`. Files from USM3D code resides in a directory named `usm3d`. The drivers of the DRAGONFLOW is located in files

```
dragon/dragon.F
dragon/dragfl.F
```

Files, which are modified to deal with flux exchange between the OVERFLOW and USM3D parts, are listed as follows:

```
usm3d/ausm.F
ns/euler/rhse.F
ns/euler/reuj.F
ns/euler/reuj2.F
ns/euler/reuk.F
```

ns/euler/reuk2.F
ns/euler/reul.F
ns/euler/reul2.F

Q values, Q_b and Q_{gh}, associated with the tetrahedral elements near the DRAGON grid interfaces need to be updated from the structured grid side. This operation has been implemented in

dragon/intface.F

Special treatment, of correcting Q values at certain nodes with IBLANK value 0, has been implemented in the following two files, for higher order cases.

ns/step/fillblk.F
ns/step/step.F

Files, which are modified to deal with viscous flux exchange between the OVERFLOW and USM3D parts, are listed as follows:

usm3d/vis513.F
ns/viscous/rhsv.F
ns/viscous/rvj.F
ns/viscous/rvj2.F
ns/viscous/rvk.F
ns/viscous/rvk2.F
ns/viscous/rvl.F
ns/viscous/rvl2.F
ns/viscous/rvjk.F
ns/viscous/rvjk2.F
ns/viscous/rvjl.F
ns/viscous/rvjl2.F
ns/viscous/rvkl.F
ns/viscous/rvkl2.F

4.2 Extension to the Family of Boundary Conditions in the OVERFLOW

An enhancement has been made to the family of boundary conditions in the OVERFLOW part, devoted to the applications such as turbomachinery. This new type of boundary condition is referred to as annular periodic condition. In this case, a convention that X axis is the reference axis to the annular periodic condition, is applied (See Figure 18). Also, it is assumed that $J - L$ planes at the ends of K direction are the corresponding planes. For an annular periodic pair (P, P') at $x = \text{const}$ and $r = \text{const}$, the periodic boundary condition requires $u_x(k = 1) = u_x(k = -1)$, $u_r(k = 1) = u_r(k = -1)$, and $u_\theta(k = 1) = u_\theta(k = -1)$. Files affected for this enhancement are listed as follows.

include/grdsav.h
grid/metjfv.F
grid/perchk.F
include/grdtop.h
grid/metric.F
grid/topchk.F

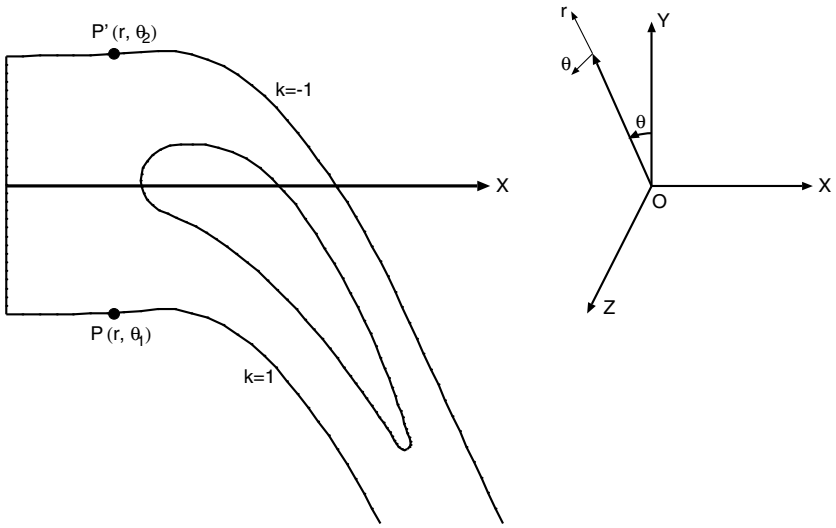

Figure 18: Diagram for the annular periodic boundary condition.

ns/bc/bc.F
ns/bc/bccopy.F
ns/control/initia.F
ns/control/parput.F
ns/mg/mgresc.F
ns/mg/mgrhsc.F
ns/mg/mgstep.F
ns/step/step.F
ns/euler/reuk.F
ns/euler/reul.F
ns/euler/rerk.F
ns/euler/fluk.F
ns/euler/dfk.F
ns/viscous/dvfk.F
ns/viscous/rhsv.F
ns/viscous/rvjk2.F
ns/viscous/rvk2.F
ns/viscous/rvkl2.F
ns/viscous/vflk.F
ns/bc/bcchek.F
ns/bc/bcper.F
ns/control/parget.F
ns/mg/forcfn.F
ns/mg/mgresf.F
ns/mg/mgrhsf.F
ns/step/rhs.F
ns/euler/rhse.F
ns/euler/reuk2.F
ns/euler/reul2.F
ns/euler/rerk2.F
ns/euler/qflrk.F
ns/viscous/dvfjk.F
ns/viscous/dvfkl.F
ns/viscous/rvjk.F
ns/viscous/rvk.F
ns/viscous/rvkl.F
ns/viscous/vfljk.F
ns/viscous/vflkl.F

5 Benchmark Tests

5.1 Shock Tube Problem

First, a 2D shock tube problem was considered. To focus only on the issue of grids, the flow was solved by the basic first-order accurate discretization in both time and space. This case serves to show the effect of interpolation in the Chimera grid and the validity of the DRAGON grid method for a transient problem as a plane shock moves across the embedded-grid region. The shock wave is moving into a quiescent region in a constant-area channel with a designed shock speed $M_s = 4$. Solutions were obtained using three grid systems, namely (1) single grid, (2) Chimera grid, and (3) DRAGON grid, as displayed in Figure 19. The single grid solution is used for benchmark comparison.

The pressure distributions along the centerline of the channel, as plotted in Figure 20, shows that the Chimera scheme predicts a faster moving shock in the tube, while the present DRAGON grid and the single grid results coincide, indicating that the shock is accurately captured and conservation property well preserved when going through the region of the embedded DRAGON grid.

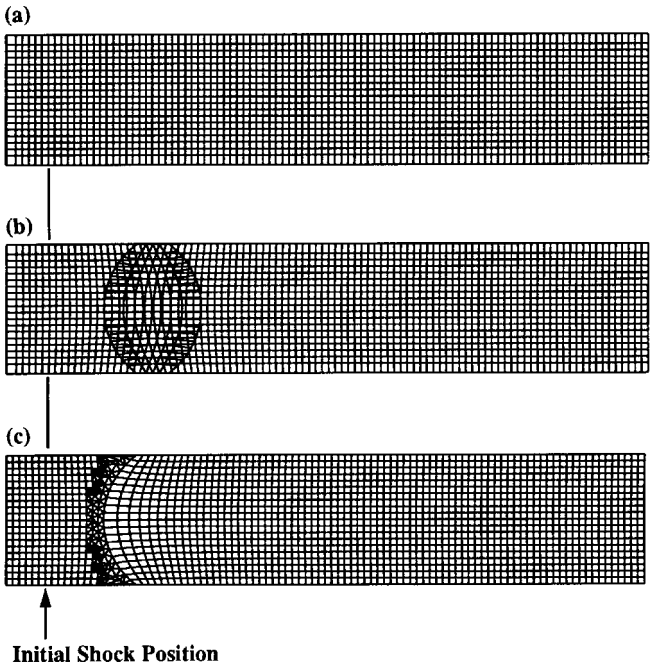

Figure 19: Grids for moving shock problem ($M_s = 4$): (a) single grid, (b) Chimera grid, and (c) DRAGON grid.

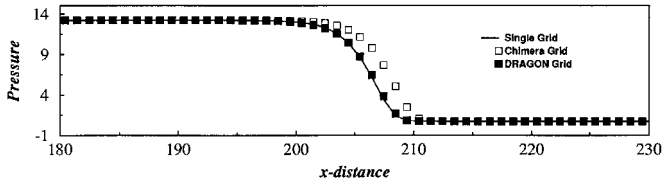

Figure 20: Comparison of centerline pressures from the three grids.

5.2 2D Supersonic Flow in a Symmetric Convergent Channel

Now we consider a supersonic flow of Mach 1.8 through a symmetric convergent channel. The configuration and pressure pattern are sketched in Figure 21, where both the top and bottom walls are bent, thus creating two wedge shocks of equal strength. The wedge angle is sufficiently large so that there is a Mach stem after the interaction of the two wedge shocks, resulting in a subsonic flow there. However, the exit flow is still supersonic, due to the acceleration of the fans emitting from the shoulders of the steps.

This test case is designed to provide a comparison in terms of conservation property between Chimera and DRAGON grids. The problem has been solved by using a single grid, two Chimera grids and a DRAGON grid, respectively. This configuration is treated as a three-dimensional geometry. Grids are generated to fill the whole domain, although the geometry is symmetric. Figure 22(a) depicts the pressure contours of the flow computed based on the single grid. Figures 22(b) and 22(c) show those computed based on two Chimera grids, I and II. The Chimera Grids I and II have the same grid point distributions as the single grid, apart from the overlapping areas. The nodal points in the overlapping areas are modestly displaced from those identical to the single grid. The difference between the Chimera Grids I and II is due to the locations of the overlapping areas. Chimera Grid II shown in Figure 22(c) is constructed in such a way that a segment of shock almost lies on one of the grid boundary. This could be the worst case that causes a large error in the simulation. However, Chimera Grid I shown in Figure 22(b) could be considered as a typical one for general applications of Chimera grids. Figure 22(d) depicts the pressure contours of the flow computed based on a DRAGON grid. This DRAGON grid is constructed based on Chimera Grid II, and a segment of shock almost lies on the DRAGON grid interface. In Figure 22(d), the contours are plotted based on the original structured grids and the corresponding unstructured grid forming the DRAGON grid. Therefore, there are discontinuities in the contour plot near the DRAGON grid interface, as there are gaps of a half cell size between the original structured grids and the unstructured grid.

Figure 23 presents the computed pressure distributions on Lines AB and CD, referring to Figure 21. It confirms that variable interpolation between grids of a Chimera grid causes the loss of conservative property, and could introduce globally significant errors in some cases. However, the DRAGON grid scheme overcomes this shortcoming.

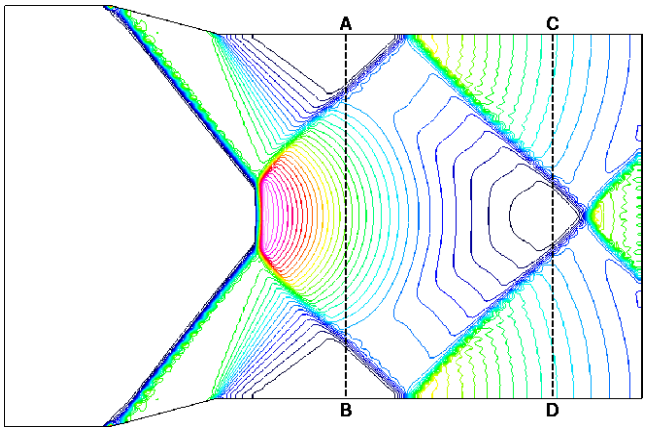

Figure 21: Geometry and pressure pattern of a symmetric convergent channel, through which a supersonic flow is passing.

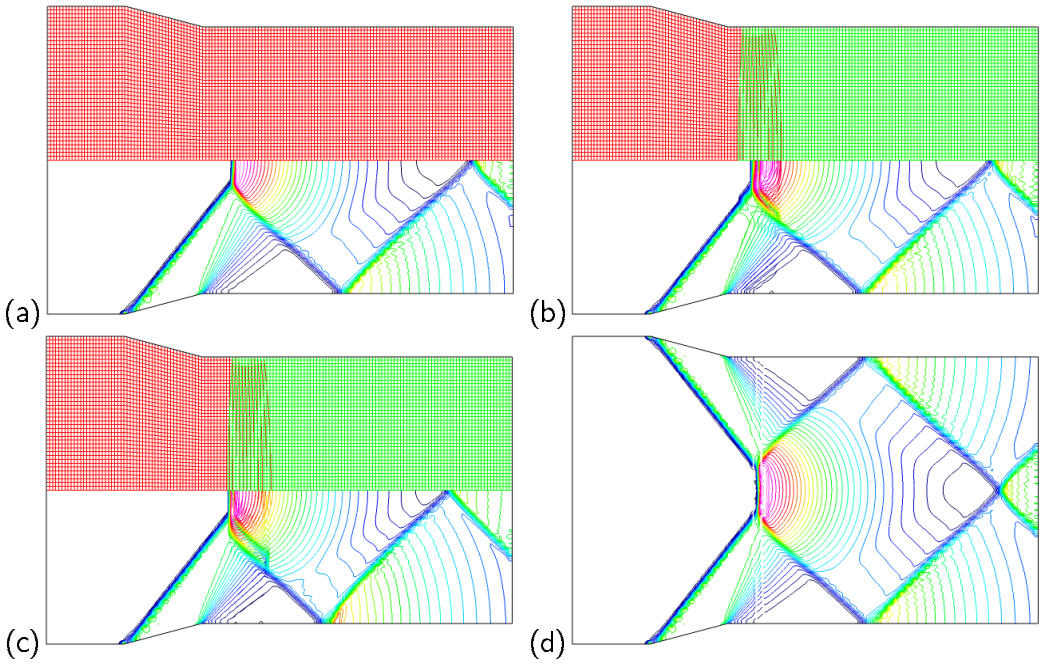

Figure 22: Pressure contours of the flow: (a) Single grid; (b) and (c) Chimera Grids I and II. (d) DRAGON grid.

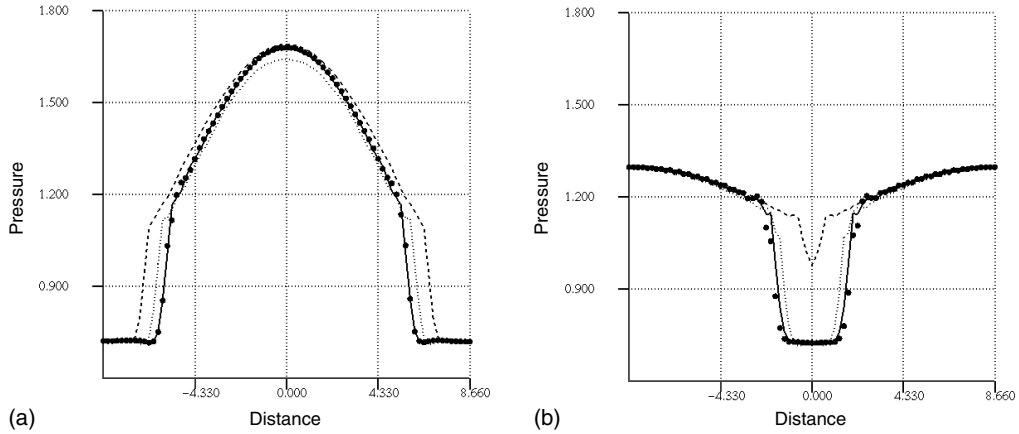

Figure 23: Pressure distributions of the flow on Lines AB (a) and CD (b), referring to Figure 21. Solid, dotted, dashed lines and circles denote results based on the single grid, Chimera Grids I and II, and the DRAGON grid, respectively.

5.3 3D Supersonic Flow in a Convergent Duct with Two Bent Side Walls

Next we consider a supersonic flow of Mach 3 through a convergent channel. The geometry is sketched in Figure 24, where both the top and front side walls are bent by a wedge angle of 10 degrees, thus creating two wedge shocks of equal strength and subsequent interactions between them. A strip of unstructured-gridded region, denoted by the shaded region, is placed in the mid-section of the channel. This test case is designed to provide a check on the three-dimensional code against conservation property of the DRAGON grid through a shock. The flow consists of two planar wedge shocks, two embedded shocks, a corner shock and two shear lines (slip surfaces) as shown in Figure 25, where the location of Section IJKL is depicted in Figure 24. The two wedge shocks intersect and generate, near the corner edge AD (see Figure 24), a corner shock region manifested by the slip surfaces emanating from the triple point. Figure 26 displays the density contours on the top and front side faces, and the exit plane. As seen in Figures 27 and 28, the corner shock region progressively becomes larger as the wedge shocks sweep towards the opposite walls. Eventually these two wedge shocks reflect and interact with the flow previously generated by the corner shocks, making the flow field even more complicated.

In Figures 29, 30 and 31, we give an inside view of variables on two planes: density contours on the symmetric plane ABCD (as denoted in Figure 24), and Mach number and pressure contours on the midplane EFGH. This reveals quite a rich feature of shock-shock interactions inside the duct, while the shock configuration on the duct walls (Figure 26) is relatively simple. The slip surfaces issuing from the shock triple points are evident in Figure 30 and they subsequently interact with the downstream shock.

It is evident that the shock profiles pass through the DRAGON grid interfaces seamlessly without creating spurious waves, guaranteeing the conservation property. In each of the above figures, we also include the results based on a single structured grid for validation. We see that both sets of results are essentially the same, except some minute variations in the core region, which are a remanent result of the unstructured grid. This is clearly indicated in Figure 29 where the shock becomes thinner in the unstructured grid region because the grid size is reduced roughly by $\frac{1}{6}$. A quantitative measure of the difference between the single grid and DRAGON grid solutions at the exit plane is given in Figure 32, indicating a close agreement of the two solutions.

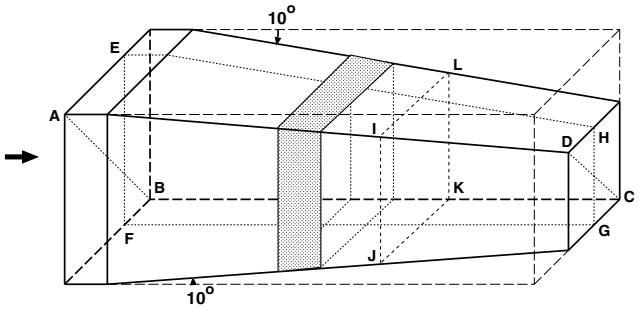

Figure 24: Sketch of a convergent duct where the unstructured grid is in the shaded region for the DRAGON grid.

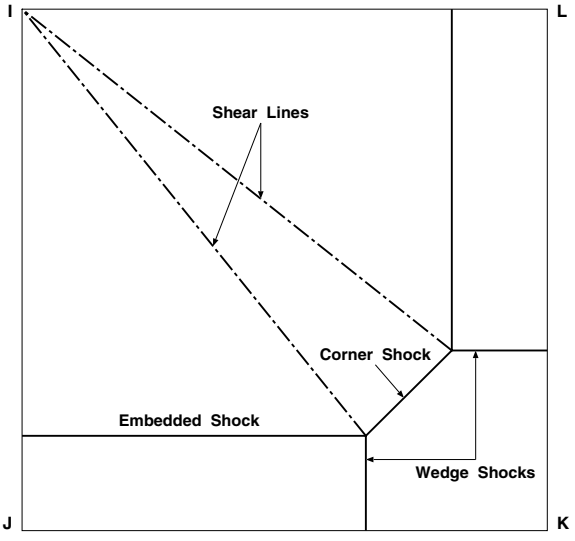

Figure 25: Flow structure in Section IJKL of the supersonic flow passing a convergent duct.

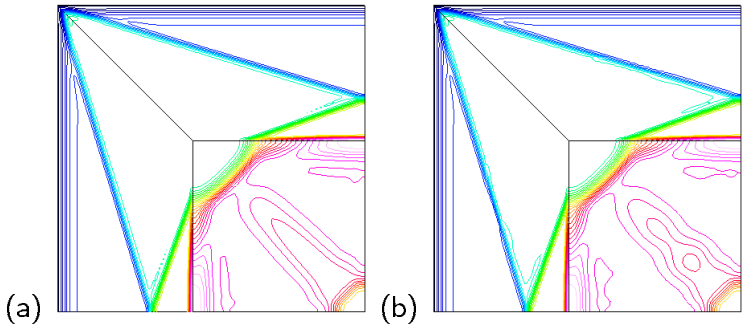

Figure 26: Density distributions of the flow on the surface of the convergent duct: (a) Single grid; (b) DRAGON grid.

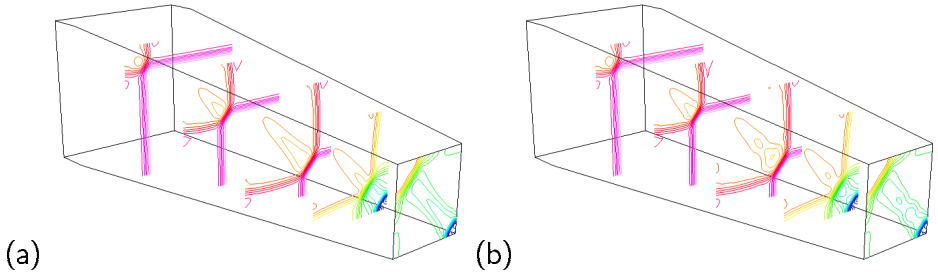

Figure 27: Mach number distributions of the flow at various stations: (a) Single grid; (b) DRAGON grid.

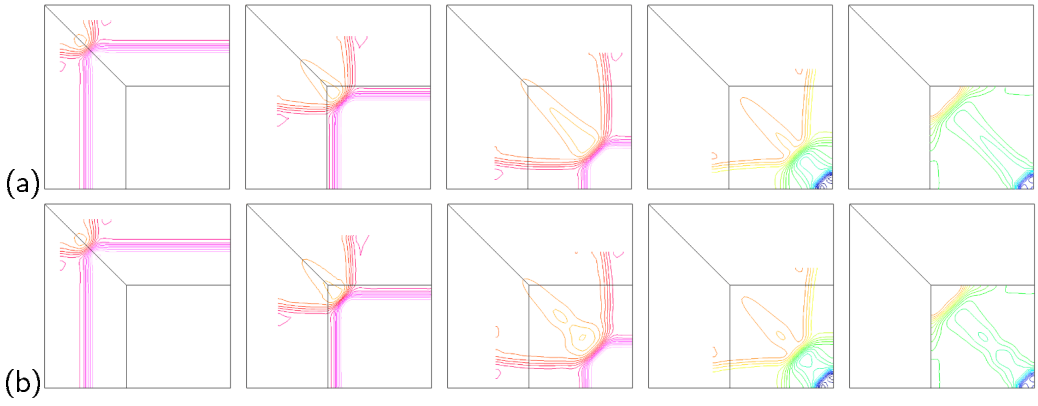

Figure 28: Mach number distributions of the flow at various stations (split view): (a) Single grid; (b) DRAGON grid.

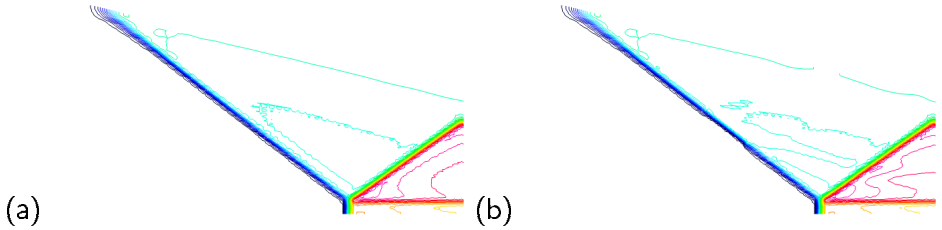

Figure 29: Density distributions of the flow at the symmetric plane ABCD: (a) Single grid; (b) DRAGON grid.

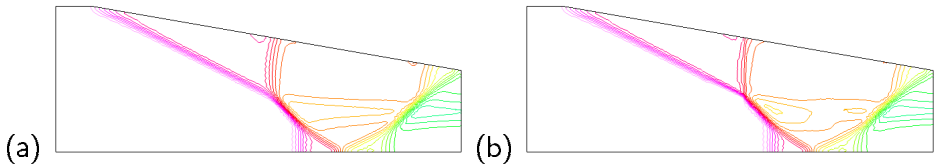

Figure 30: Mach number distributions of the flow at a typical cutting plane EFGH: (a) Single grid; (b) DRAGON grid.

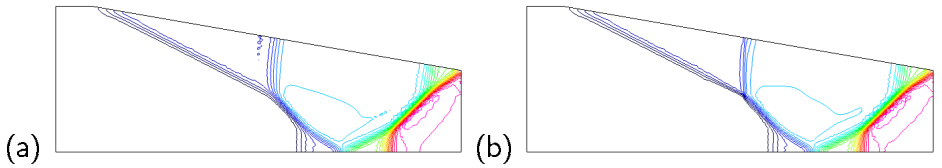

Figure 31: Pressure distributions of the flow at a typical cutting plane EFGH: (a) Single grid; (b) DRAGON grid.

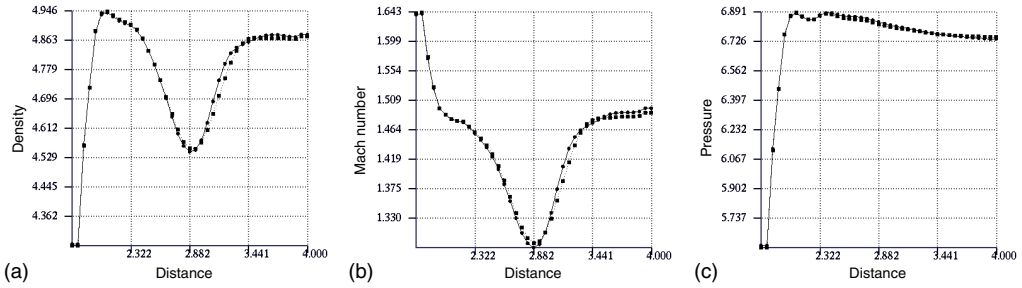

Figure 32: (a) Density, (b) Mach number and (c) pressure distributions of the flow on Line HG. Boxes and circles denote results based on the single grid and the DRAGON grid, respectively.

5.4 Subsonic Flow through a Wavy-Wall Duct

We consider a subsonic flow in a wavy-wall duct, of which the problem setting is illustrated in Figure 33. This test case is designed to provide a check on the three-dimensional code against conservation property of the DRAGON grid for a subsonic flow. We have performed computational simulation based on a single grid and a DRAGON grid, respectively. The DRAGON grid has unstructured grid regions of a shape as Label "3D", and the geometry is sketched in Figure 34. Figure 35 provides additional views of the DRAGON grid. As the result, Figures 36, 37, and 38 depict the density, Mach number and pressure distributions for both cases based on the single grid and the DRAGON grid. It is evident that the results of both cases are essentially the same. The flow passes through the DRAGON grid interfaces seamlessly without creating spurious diffusion, and this guarantees the conservation property.

And further, Figure 39 shows a quantitative measure of the difference between the single grid and DRAGON grid solutions on lines AB and CD, which are defined in Figure 34. This figure indicates a close agreement of the two solutions in terms of density, Mach number and pressure distributions.

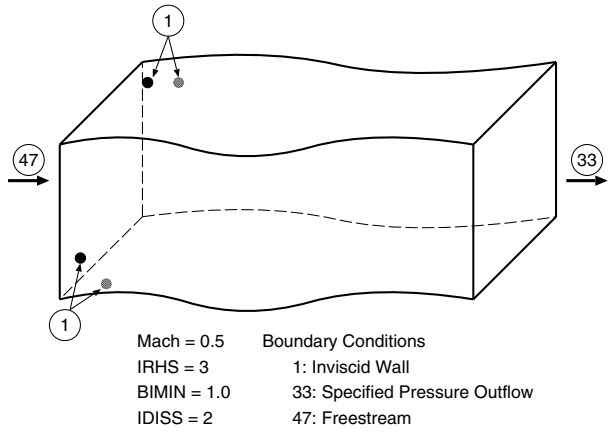

Figure 33: Problem setting of flow in the wavy-wall duct.

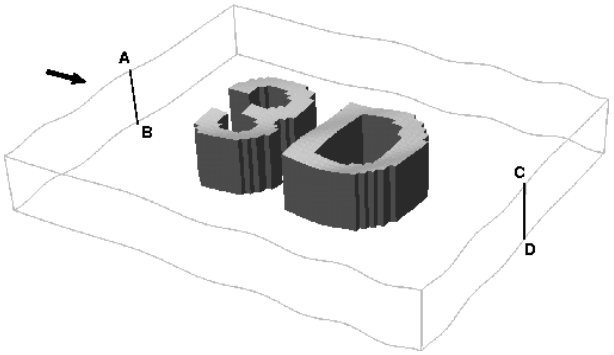

Figure 34: Sketch of a wavy-wall duct where the unstructured grid is in the shaded region for the DRAGON grid.

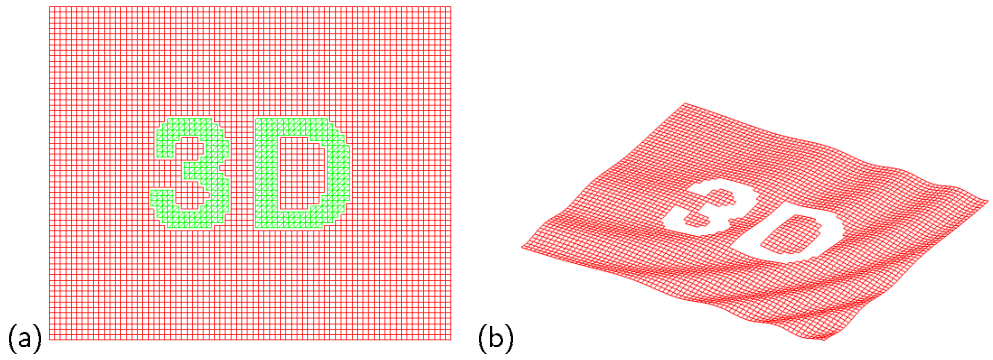

Figure 35: (a) a view of the DRAGON grid; (b) A layer of the structured grid in the DRAGON grid.

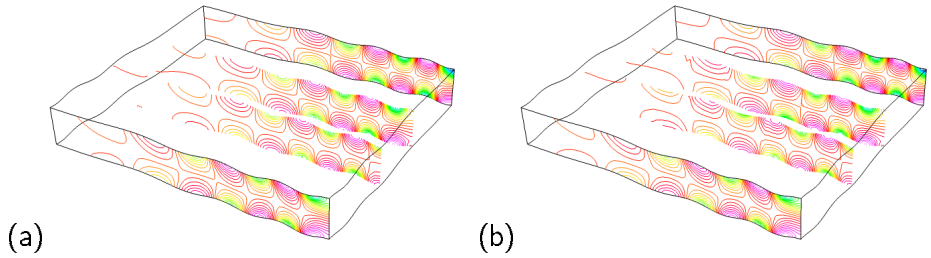

Figure 36: Density distributions of the flow in the wavy-wall duct: (a) Single grid; (b) DRAGON grid.

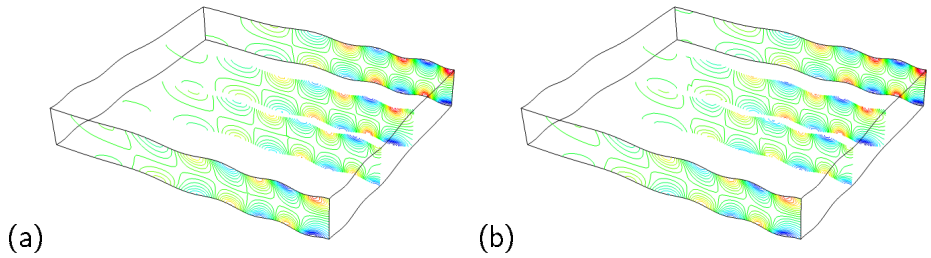

Figure 37: Mach number distributions of the flow in the wavy-wall duct: (a) Single grid; (b) DRAGON grid.

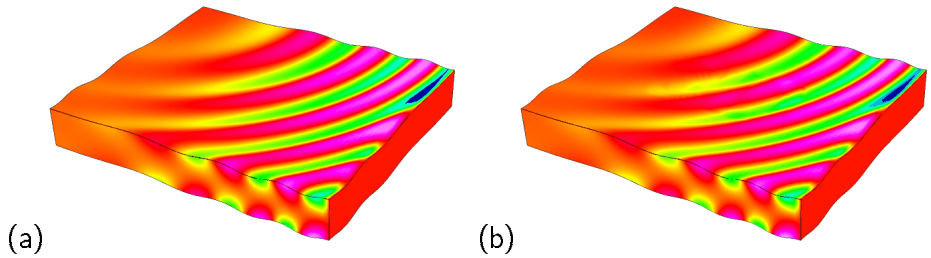

Figure 38: Pressure distributions of the flow on the surface of the wavy-wall duct: (a) Single grid; (b) DRAGON grid.

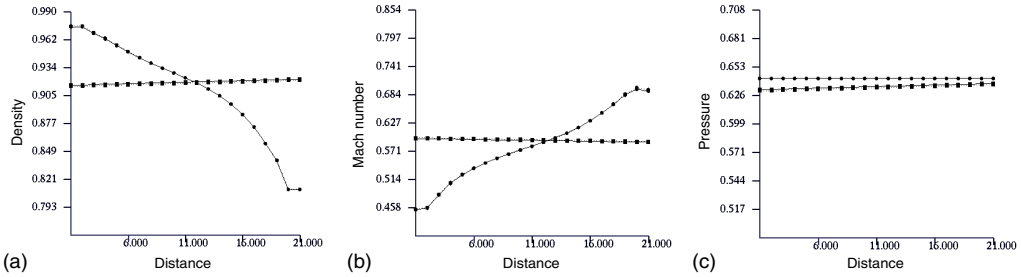

Figure 39: (a) Density, (b) Mach number and (c) pressure distributions of the flow on Lines AB (boxes) and CD (circles). Doted and solid lines denote results based on the single grid and the DRAGON grid, respectively.

6 Numerical Simulations

6.1 Inviscid Flow around a Linear Cascade

We have conducted a 3D calculation of an inviscid flow around a cascade in a turning duct. This solution exhibits the capability of DRAGON grid scheme in dealing with problems involving complex geometries. Also calculation based on a Chimera grid, which is the base grid of the DRAGON grid, has been conducted in order to make a comparison. Figure 40 illustrates the 3D DRAGON and Chimera grids for the computational domain of concern, and Figure 41 shows the unstructured grid of the corresponding DRAGON grid. Figures 42, 43 and 44 depict the pressure, density and Mach number contours of the solutions. Finally Figure 45 shows the pressure distributions on the surfaces of the six vanes, where (a), (b), (c), (d), (e) and (f) are for the first to last vanes from the center outwards, respectively. While no measurements are available for comparison, both Chimera and DRAGON grid solutions, at least serving as a code-to-code validation, are in agreement with each other, especially on the pressure side of the vanes. But there are noticeable differences on the suction side of the vanes. From the contour plots, Figures 42-44, The DRAGON grid solutions appear to be smoother and free of noises emanating from the interpolation surfaces.

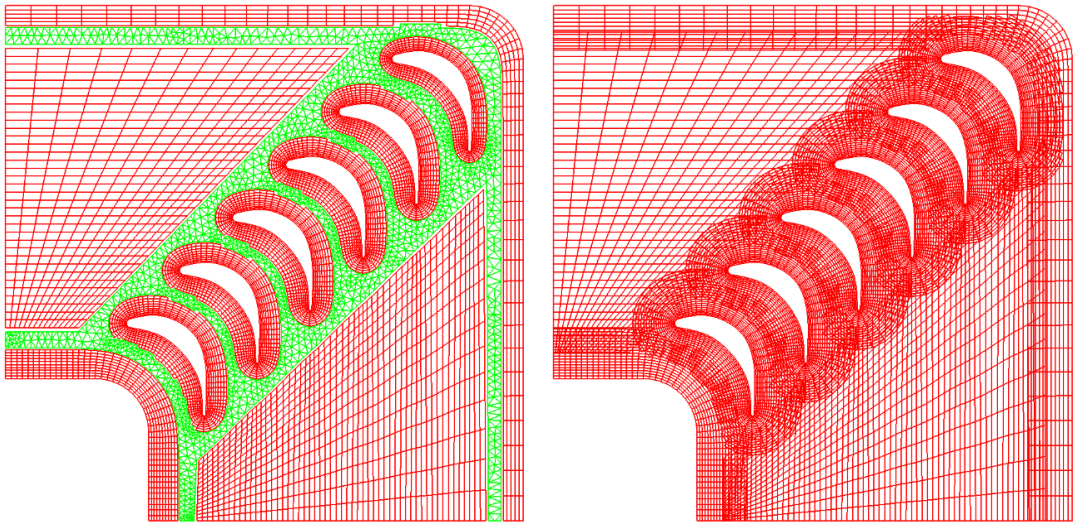

Figure 40: 3D DRAGON and Chimera grids of the cascade.

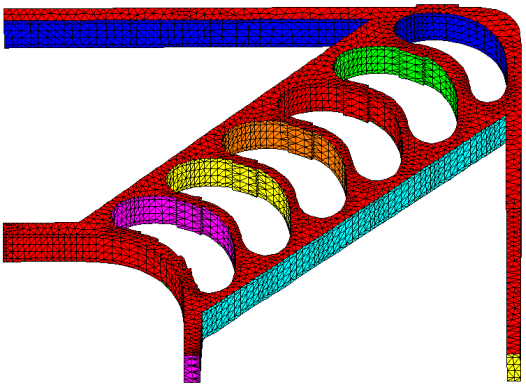

Figure 41: Unstructured grid of the DRAGON grid of the cascade.

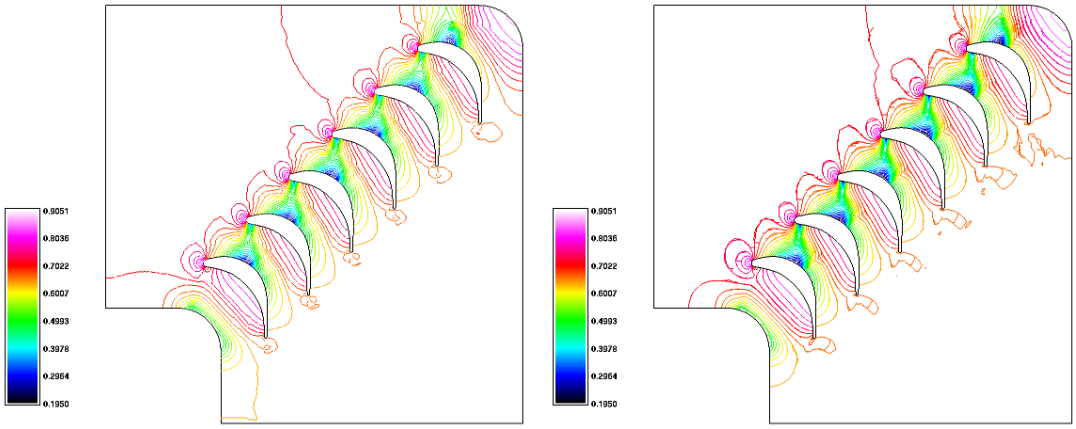

Figure 42: Pressure distributions of solutions based on the DRAGON and Chimera grids.

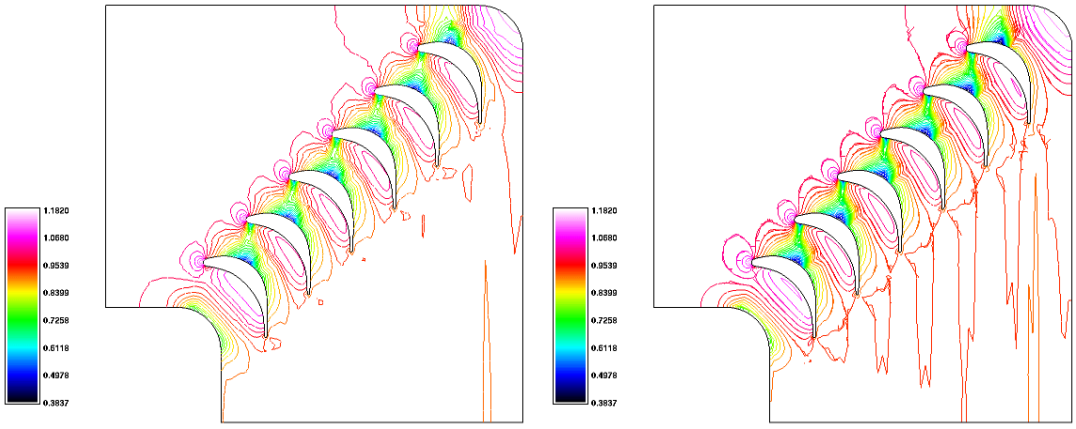

Figure 43: Density distributions of solutions based on the DRAGON and Chimera grids.

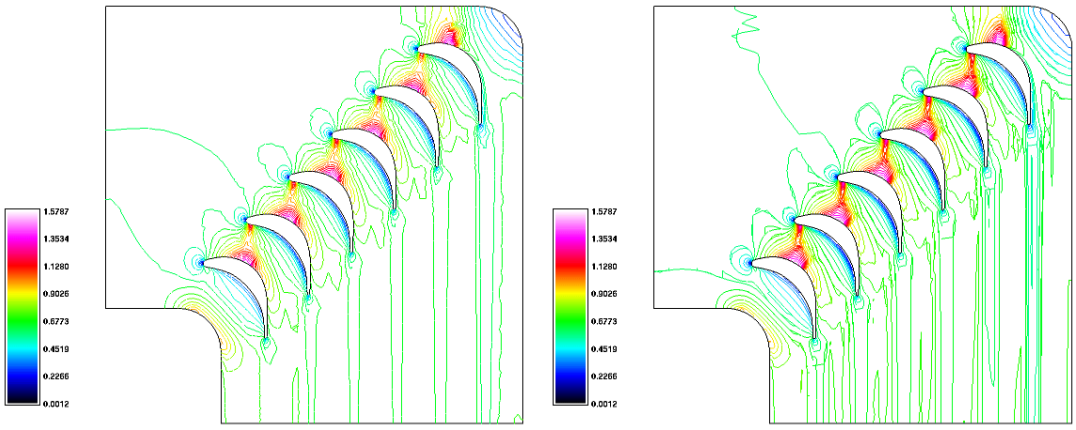

Figure 44: Mach number distributions of solutions based on the DRAGON and Chimera grids.

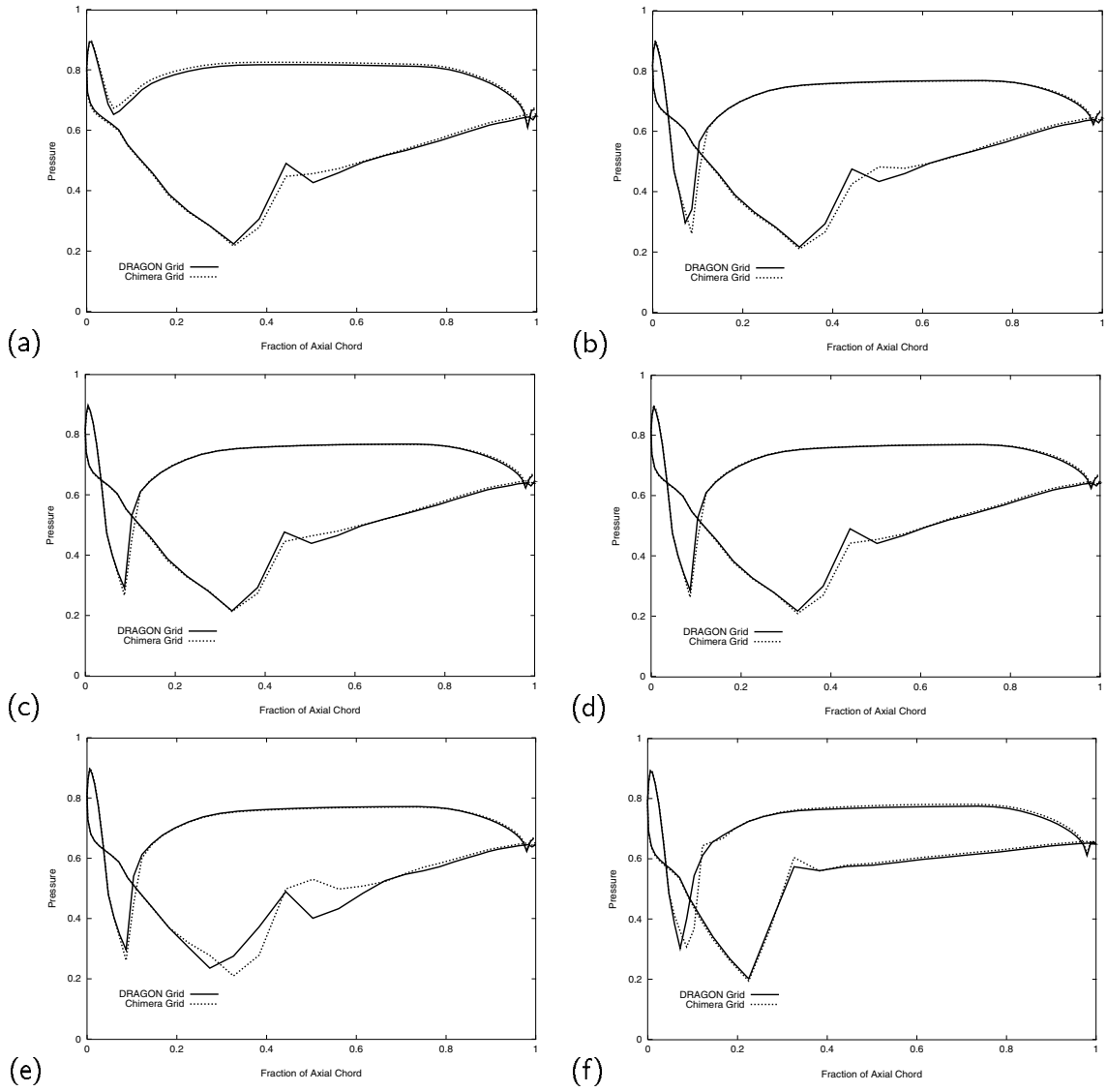

Figure 45: Pressure distributions around the six vanes: (a), (b), (c), (d), (e) and (f) are for the first to last vanes from the center outwards, respectively.

6.2 Viscous Flow through an Annular Cascade

Lastly, we show the results of a flow simulation for an annular cascade of turbine stator vanes developed and tested at NASA Lewis [6]. The annular ring has 36 untwisted vanes, of constant profile from hub to tip, with a hub-tip radius ratio of 0.85 and a tip diameter of 508 mm. The vanes themselves are 38.10mm high, and have an axial chord of 38.23mm and a blade chord of 55.52mm (See Figure 46). Design flow conditions are for a fully axial inflow with an exit-hub-static to inlet-total pressure ratio of 0.6705. The designed inflow Mach number is 0.2. The Reynolds number based on the axial chord is 1.73×10^5[3], or 4.52524×10^6 in a unit of meter used as an input value for the solver. These conditions correspond to average inlet and exit Mach numbers of 0.211 and 0.697, respectively. However, as in [3] we assume the free stream Mach number of 0.2 in the calculation.

A DRAGON grid as shown in Figures 47 and 48 is used for the flow simulation. It consists of a background H-type grid placed to cover the channel between the vanes, an O-type viscous grid used to resolve the region around the vane, and an unstructured grid (See Figure 49) located in the overlapping region between the H- and O-type grids. The H-type grid has $60 \times 31 \times 33$ points, and O-type grid $85 \times 20 \times 33$ points. All the three component grids have viscous layers near the hub and the tip. The initial spacing at the wall is 0.0002 of a blade chord, that is, 0.0111mm.

Previous calculations have been obtained using a single structured grid [2, 3]. The computed surface static pressure distributions of the present DRAGON grid solution are plotted in Figure 50, and they are seen to be in very good agreement with the measured data [6] at three spanwise locations, 13.3%, 50%, and 86.6%, respectively. Note that the plot shown in Figure 50 has been scaled with respect to the inlet-total pressure P_0. Figure 51 depicts the pressure contours on the vane surfaces and on the hub. The pressure side displays a basically two-dimensional behavior while a significant spanwise variation is seen on the suction side.

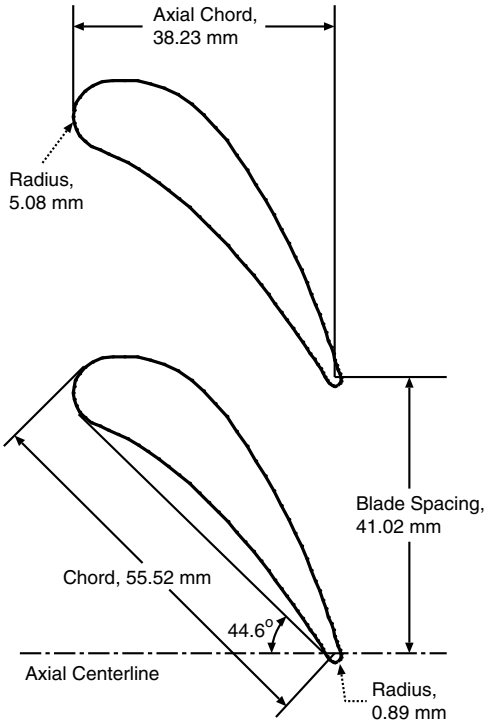

Figure 46: Core turbine stator vane geometry at the mean section.

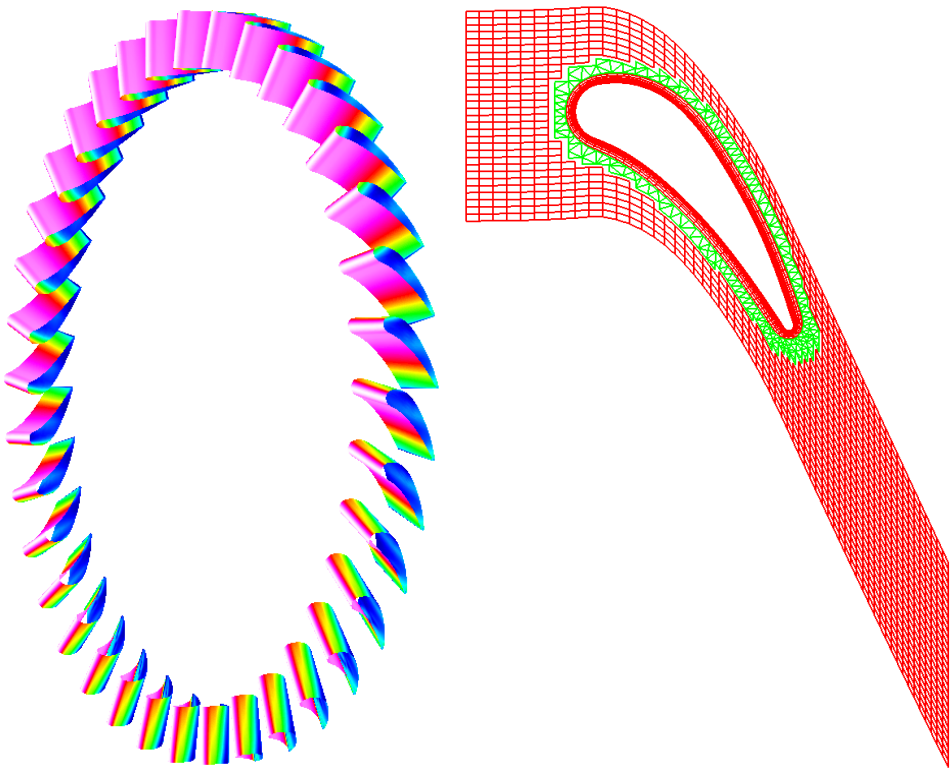

Figure 47: 3D DRAGON grid for a turbine vane.

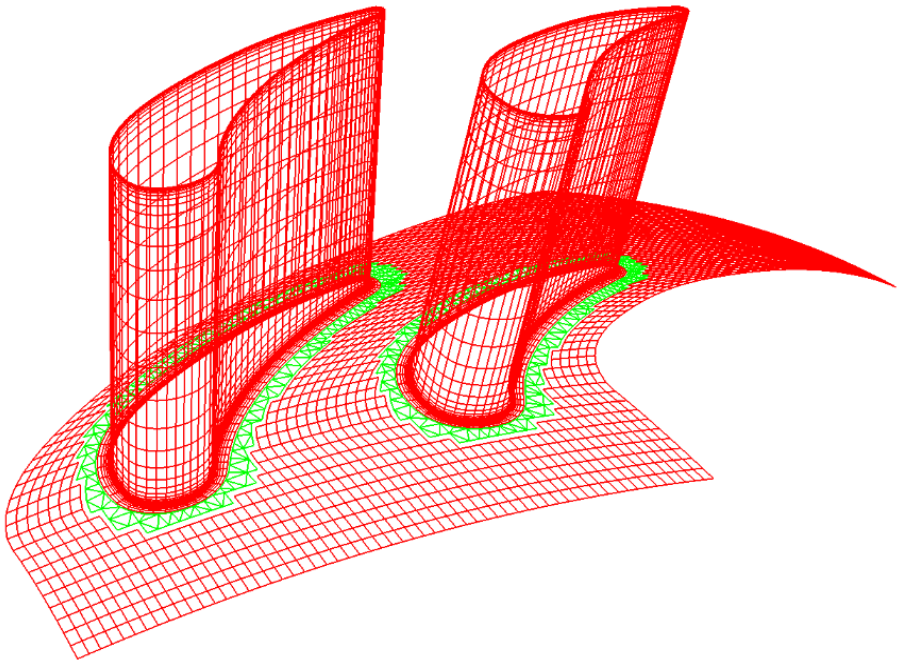

Figure 48: DRAGON grid of the annular turbine cascade.

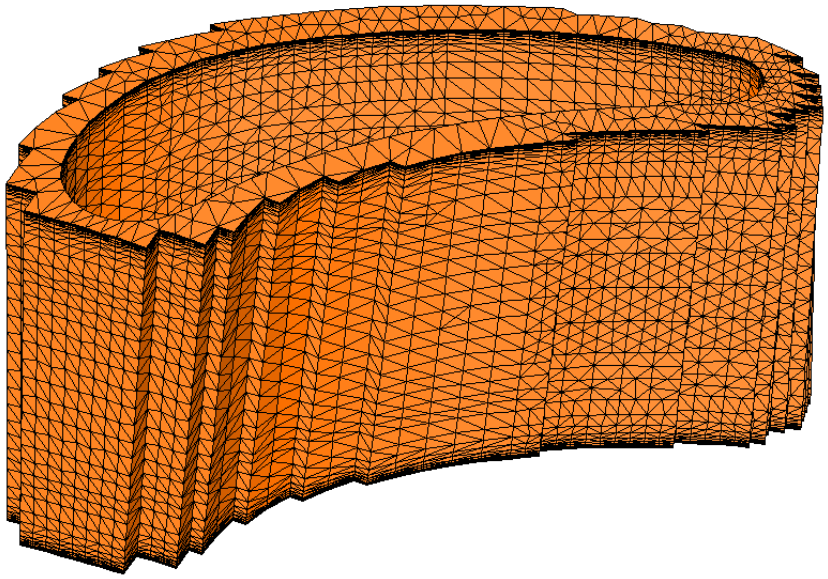

Figure 49: Unstructured grid of the corresponding DRAGON grid.

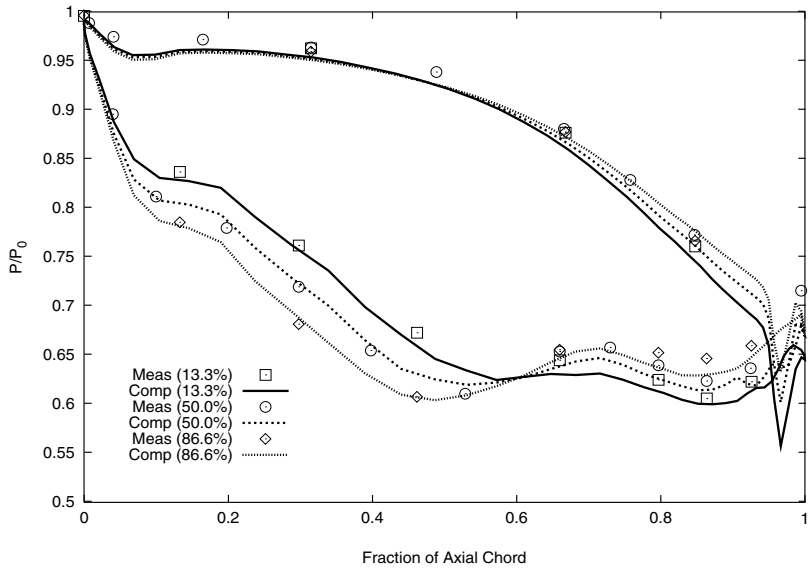

Figure 50: Computed and measured static pressure distributions at 13.3%, 50% and 86.6% of span from hub.

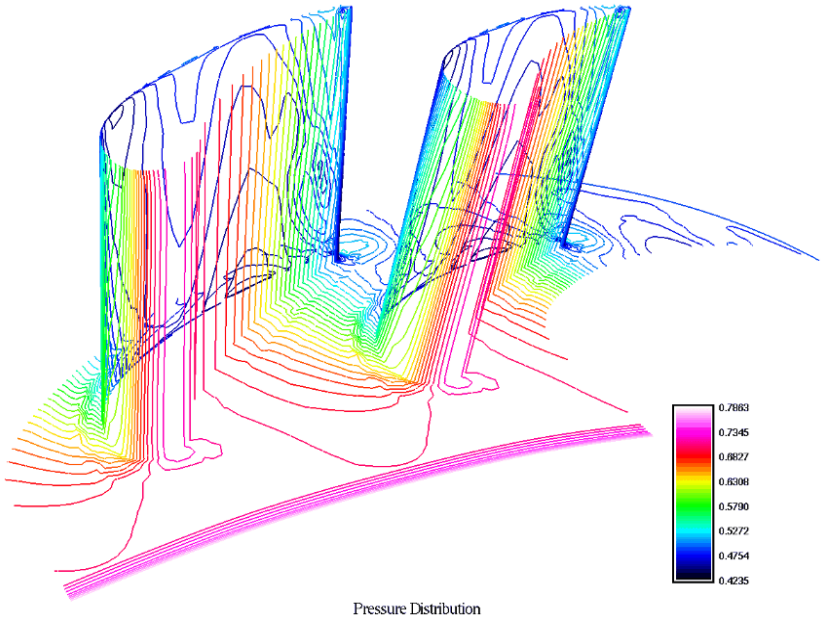

Figure 51: Pressure distribution for the annular turbine cascade showing two vanes.

7 Concluding Remarks

In the present work, we have concentrated on the extension of the DRAGON grid method into three-dimensional space. This method attempts to preserve the advantageous features of both the structured and unstructured grids, while eliminating or minimizing their respective shortcomings. The flow solutions confirm the satisfaction of conservation property through the interfaces of structured-unstructured regions, and the results are in very good agreement with the measured data, thus demonstrating the reliability of the method. Future plan includes further validations and applications to engineering problems with complex geometry.

Appendix

File Descriptions

For the execution of the DRAGONFLOW code, information on topology relation between the two types of grids near the DRAGON grid interface is required. This information is provided through a set of four files, that is, `*.fls`, `*.fdef`, `*.fcm` and `*.pcm`.

File `*.fls` provides information on face list numbers. Its file format is as follows:

```
NGRID_STR
DO IG=1,NGRID_STR
  JDIM(IG),KDIM(IG),LDIM(IG)
  DO II=1,LDIM(IG)
    NFFLS=NFFLS+1
    II,LFFLS(NFFLS)
  ENDDO
  DO II=1,LDIM(IG)
    NFFLS=NFFLS+1
    II,LFFLS(NFFLS)
  ENDDO
  DO II=1,KDIM(IG)
    NFFLS=NFFLS+1
    II,LFFLS(NFFLS)
  ENDDO
ENDDO
Note:
  LFFLS(*)    --- numbers of quadrilateral faces in i, j, and
                  k-directions, respectively. The faces are grouped
                  according to loops DO II=1,LDIM(IG), DO II=1,LDIM(IG)
                  and DO II=1,KDIM(IG).
```

Face definition file *.fdef provides definition information for DRAGON interfaces. Every interface can be defined as $(i, j, k;\text{idir})$ as shown in Figure 5. The file format is as follows:

```
  NSURF
  DO IS=1,NSURF
    ISURQ,(LFDEF(IS,IM),IM=1,5)
  ENDDO
Notes:
  ISURQ       --- overall numbering of quadrilateral faces;
  LFDEF(IS,1) --- i;
  LFDEF(IS,2) --- j;
  LFDEF(IS,3) --- k;
  LFDEF(IS,4) --- idir (1, -1, 2, -2, 3, -3); and
  LFDEF(IS,5) --- ig_str;
```

File *.fcm provides information on face couple mapping. Its file format is as follows:

```
  NSURQ_I,NSURT_I
  DO J=1,NSURQ_I
    (LFFCM(J,IM),IM=1,4)
  ENDDO
  DO J=1,NSURT_I
    LFVCT(J)
  ENDDO
Notes:
  LFFCM(J,1)  --- index of the quadrilateral face.
                  NSURQ faces are ordered according to the *.fdef file.
  LFFCM(J,2)  --- ID of an unstructured volume grid.
  LFFCM(J,3)  --- starting index of slave (triangular) faces.
  LFFCM(J,4)  --- ending index of slave (triangular) faces.
  LFVCT(J)    --- a pointer to overall face list.
                  That is ID of a slave face.
```

Point couple mapping file *.pcm provides information on point couple mapping on DRAGON interfaces, with respect to fictitious grids. The file format is as follows:

```
  NPSURQ
  DO IP=1,NPSURQ
    IP,IPTET,IG_UNS,IG_STR,J,K,L
  ENDDO
Notes:
  NPSURQ      --- Number of points on quadrilateral DRAGON interface.
  IP          --- index of the point on quadrilateral DRAGON interface.
  IPTET       --- index of surface point of the unstructured grid.
  IG_UNS      --- unstructured grid ID.
  IG_STR      --- structured grid ID.
  J,K,L       --- definition of the point in the fictitious grid.
```

Generation of Relation Files

Four auxiliary files are used for creating information contained in Files *.fls, *.fdef, *.fcm and *.pcm. These files are named as *.fat, *.pat, *.pcm0 and *.vis.

Face attribution file *.fat provides information on attributions of DRAGON interfaces. Every triangular face can be defined as (v_1, v_2, v_3), and the file format is as follows:

```
NSURT
DO IS=1,NSURT
  IS,V1,V2,V3,BCID,PATCHID,ISDRAGON
ENDDO
Notes:
  V1,V2,V3    --- definition of a triangular face. The nodal numbering
                  is based on the surface triangulation.
  BCID        --- boundary type.
  PATCHID     --- patch ID, which is the index of a quadrilateral face.
  ISDRAGON    --- flag indicating whether the face is on
                  the DRAGON interface.
```

Point attribution file *.pat provides information about attributions of points on DRAGON grid interfaces, with respect to fictitious grids. The file format is as follows:

```
NPSURQ
DO IP=1,NPSURQ
  IPSURQ,IG_STR,J,K,L
ENDDO
Notes:
  NPSURQ      --- Number of points on quadrilateral DRAGON interface.
  IPSURQ      --- index of the point on quadrilateral DRAGON interface.
  IG_STR      --- structured grid ID.
  J,K,L       --- definition of the point in the fictitous grid.
```

Note that faces are grouped according to their parents, that is, patchids.

Initial point couple mapping file *.pcm0 provides information on point couple mapping on DRAGON interfaces. The file format is as follows:

```
NPSURQ
DO IP=1,NPSURQ
  IPTET,IPSURQ
ENDDO
Notes:
  NPSURQ      --- Number of special points on the surface of the unstructured
                  grid, which match to points on quadrilateral DRAGON interface
                  (NPSURQ = NPSUR_TET).
  IPTET       --- index of surface point of the unstructured grid.
  IPSURQ      --- index of the point on quadrilateral DRAGON interface.
```

For cases with viscous flows involved, viscous layers can be generated based on an intermediate unstructured grid. In these cases, additional information is required, which is written in a viscous layer information file *.vis. The file format is as follows:

```
NPSURQ_I,NSURQ_I
DO IS=1,NSURQ_I
  ISMAP
ENDDO
DO IP=1,NPSURQ_I
  COORQ(1),COORQ(2),COORQ(3)
ENDDO
DO IP=1,NPSURQ_I
  (IPATT(J),J=1,4)
```

```
  ENDDO
Notes:
  NPSURQ_I    --- Number of points on quadrilateral DRAGON interface.
  NSURQ_I     --- Number of patches on quadrilateral DRAGON interface.
  ISMAP       --- Numbering index of surface patches. The numbering
                  splits patches into groupes, which correspond to
                  areas of unstructured grids and viscous layers.
                  The former is with positive indices while the
                  later negtive indices.
  COORQ(*)    --- Coordinates of points on quadrilateral DRAGON interface.
  IPATT       --- Attribution of the points on quadrilateral DRAGON interface
                  (IG_STR,J,K,L)
```

References

[1] P. G. Buning and et. al. OVERFLOW user's manual, version 1.8f. Unpublished NASA report, NASA, 1998.

[2] R. V. Chima, P. W. Giel, and R. J. Boyle. An algebraic turbulence model for three-dimensional viscous flows. NASA TM 105931, NASA, 1993.

[3] R. V. Chima and J. W. Yokota. Numerical analysis of three-dimensional viscous internal flows. NASA TM 100878, NASA, 1988.

[4] N. T. Frink. Upwind scheme for solving the Euler equations on unstructured tetrahedral meshes. *AIAA Journal*, 30(1):70–77, 1992.

[5] N. T. Frink. Tetrahedral unstructured Navier-Stokes method for turbulent flows. *AIAA Journal*, 36(11):1975–1982, 1998.

[6] L. J. Goldman and R. G. Seasholtz. Laser anemometer measurements in an annular cascade of core turbine vanes and comparison with theory. NASA Technical Paper 2018, NASA, 1982.

[7] D. G. Holmes and S. D. Connell. Solution of the 2D Navier-Stokes equations on unstructured adaptive grids. AIAA Paper 89-1932, AIAA 9th CFD Conference, Buffalo, NY, June 1989.

[8] K.-H. Kao and M.-S. Liou. Advance in overset grid schemes: From Chimera to DRAGON grids. *AIAA Journal*, 33(10):1809–1815, 1995.

[9] B. Koren. Upwind schemes, multigrid and defect correction for the steady Navier-Stokes equations. In *Lecture Notes in Physics*, volume 323, pages 344–348. 1989.

[10] A. Lerat and Z. N. Wu. Stable conservative multidomain treatments for implicit Euler solvers. *Journal of Computational Physics*, 123:45–64, 1996.

[11] M.-S. Liou. A continuing search for a near-perfect numerical flux scheme, Part I: AUSM$^+$. NASA TM 106524, Lewis Research Center, Cleveland, Ohio, 1994. Also *Journal of Computational Physics*, 129: 364–382, 1996.

[12] M.-S. Liou. Numerical speed of sound and its application to schemes for all speeds. AIAA Paper 99-3268-CP, 14th AIAA CFD Conference, 1999.

[13] M.-S. Liou and K.-H. Kao. Progress in grid generation: From Chimera to DRAGON grids. NASA TM 106709, Lewis Research Center, Cleveland, Ohio, August 1994. Also Chapter 21, in Frontiers of Computational Fluid Dynamics 1994, ed. D. A. Caughey and M. M. Hafez, John Wiley & Sons, November 1994.

[14] M.-S. Liou and C. J. Steffen. A new flux splitting scheme. *Journal of Computational Physics*, 107:23, 1993.

[15] M.-S. Liou and Y. Zheng. Development of 3D DRAGON grid method for complex geometry. In D. A. Caughey and M. M. Hafez, editors, *Frontiers of Computational Fluid Dynamics – 2002*. World Scientific Publishing Company, Singapore, 2001.

[16] M.-S. Liou and Y. Zheng. A three-dimensional hybrid grid: DRAGON grid. In N. Satofuka, editor, *Computational Fluid Dynamics 2000, Proceedings of the First International Conference on Computational Fluid Dynamics (1st ICCFD) (Kyoto, Japan, July, 2000)*, pages 113–118. Springer-Verlag, Berlin, 2001.

[17] K. Nakahashi and S. Obayashi. FDM-FEM zonal approach for viscous flow computations over multiple-bodies. AIAA Paper 87-0604, AIAA 25th Aerospace Sciences Meeting, Reno, NV, January 1987.

[18] M. Soetrisno, S. T. Imlay, and D. W. Roberts. A zonal implicit procedure for hybrid structured-unstructured grids. AIAA Paper 94-0645, AIAA 32nd Aerospace Sciences Meeting & Exhibit, Reno, NV, 1994.

[19] Z. J. Wang, N. Hariharan, and R. Chen. Recent developments on the conservation property of Chimera. AIAA Paper 98-0216, AIAA 36th Aerospace Sciences Meeting & Exhibit, Reno, NV, January 1998.

[20] N. P. Weatherill. On the combination of structured-unstructured meshes. In S. Sengupta, J. Häuser, P. R. Eiseman, and J. F. Thompson, editors, *Numerical Grid Generation in Computational Fluid Mechanics*, pages 729–739, Swansea, UK, 1988. Pineridge Press.

[21] Y. Zheng and M.-S. Liou. Progress in the three-dimensional DRAGON grid scheme. AIAA Paper 2001–2540, Presented at the 15th AIAA Computational Fluid Dynamics Conference (California, USA, June, 2001), 2001.

[22] Y. Zheng, M.-S. Liou, and K. C. Civinskas. Development of three-dimensional DRAGON grid technology. NASA TM 1999-209458, NASA, November 1999.

REPORT DOCUMENTATION PAGE

Form Approved
OMB No. 0704-0188

Public reporting burden for this collection of information is estimated to average 1 hour per response, including the time for reviewing instructions, searching existing data sources, gathering and maintaining the data needed, and completing and reviewing the collection of information. Send comments regarding this burden estimate or any other aspect of this collection of information, including suggestions for reducing this burden, to Washington Headquarters Services, Directorate for Information Operations and Reports, 1215 Jefferson Davis Highway, Suite 1204, Arlington, VA 22202-4302, and to the Office of Management and Budget, Paperwork Reduction Project (0704-0188), Washington, DC 20503.

1. AGENCY USE ONLY (*Leave blank*)	2. REPORT DATE	3. REPORT TYPE AND DATES COVERED
	May 2002	Technical Memorandum

4. TITLE AND SUBTITLE

A Flow Solver for Three-Dimensional DRAGON Grids

5. FUNDING NUMBERS

WU–708–28–13–00

6. AUTHOR(S)

Meng-Sing Liou and Yao Zheng

7. PERFORMING ORGANIZATION NAME(S) AND ADDRESS(ES)

National Aeronautics and Space Administration
John H. Glenn Research Center at Lewis Field
Cleveland, Ohio 44135–3191

8. PERFORMING ORGANIZATION REPORT NUMBER

E–13298

9. SPONSORING/MONITORING AGENCY NAME(S) AND ADDRESS(ES)

National Aeronautics and Space Administration
Washington, DC 20546–0001

10. SPONSORING/MONITORING AGENCY REPORT NUMBER

NASA TM—2002-211512

11. SUPPLEMENTARY NOTES

Meng-Sing Liou, NASA Glenn Research Center, Cleveland, Ohio; and Yao Zheng, Taitech, Inc., Cleveland, Ohio 44135. Responsible person, Meng-Sing Liou, organization code 5880, 216–433–5855.

12a. DISTRIBUTION/AVAILABILITY STATEMENT

Unclassified - Unlimited
Subject Categories: 34 and 61 Distribution: Nonstandard

Available electronically at http://gltrs.grc.nasa.gov/GLTRS

This publication is available from the NASA Center for AeroSpace Information, 301–621–0390.

12b. DISTRIBUTION CODE

13. ABSTRACT ***(Maximum 200 words)***

DRAGONFLOW code has been developed to solve three-dimensional Navier-Stokes equations over a complex geometry whose flow domain is discretized with the DRAGON grid—a combination of Chimera grid and a collection of unstructured grids. In the DRAGONFLOW suite, both OVERFLOW and USM3D are presented in form of module libraries, and a master module controls the invoking of these individual modules. This report includes essential aspects, programming structures, benchmark tests and numerical simulations.

14. SUBJECT TERMS

Computational fluid dynamics; Grid generation; Turbomachinery; Turbine vanes; Cascade flow; Supersonic flow; Subsonic flow; Viscous flow

15. NUMBER OF PAGES

48

16. PRICE CODE

17. SECURITY CLASSIFICATION OF REPORT	18. SECURITY CLASSIFICATION OF THIS PAGE	19. SECURITY CLASSIFICATION OF ABSTRACT	20. LIMITATION OF ABSTRACT
Unclassified	Unclassified	Unclassified	